Development 140, 2787-2797 (2013) doi:10.1242/dev.096487

ArhGEF18 regulates RhoA-Rock2 signaling to maintain neuro-epithelial apico-basal polarity and proliferation

Cathrin Herder[1], Jakub M. Swiercz[2], Claudia Müller[3,4], Ravindra Peravali[1], Rebecca Quiring[3,5], Stefan Offermanns[2], Joachim Wittbrodt[1,3,4,*] and Felix Loosli[1,3,*,‡]

SUMMARY

The vertebrate central nervous system develops from an epithelium where cells are polarized along the apicobasal axis. Loss of this polarity results in abnormal organ architecture, morphology and proliferation. We found that mutations of the guanine nucleotide exchange factor *ArhGEF18* affect apicobasal polarity of the retinal neuroepithelium in medaka fish. We show that *ArhGEF18*-mediated activation of the small GTPase *RhoA* is required to maintain apicobasal polarity at the onset of retinal differentiation and to control the ratio of neurogenic to proliferative cell divisions. *RhoA* signals through *Rock2* to regulate apicobasal polarity, tight junction localization and the cortical actin cytoskeleton. The human *ArhGEF18* homologue can rescue the mutant phenotype, suggesting a conserved function in vertebrate neuroepithelia. Our analysis identifies *ArhGEF18* as a key regulator of tissue architecture and function, controlling apicobasal polarity and proliferation through *RhoA* activation. We thus identify the control of neuroepithelial apicobasal polarity as a novel role for *RhoA* signaling in vertebrate development.

KEY WORDS: ArhGEF18, Medaka, Retina, Rho signaling, Teleost, Epithelial polarity

INTRODUCTION

Epithelial sheets are essential for the development of many vertebrate organs, including the central nervous system and retina. Epithelial cells are highly polarized along their apicobasal (a-b) axis, which is crucial for both function and morphology of epithelia. A-b polarity is established and maintained by three major protein complexes: Par and Crumbs complexes are required for apical membrane identity, whereas the Scribble complex antagonizes them more basally, thus conferring basolateral identity (Royer and Lu, 2011).

Small GTPases of the Rho family function as molecular switches in a wide range of cellular processes (Heasman and Ridley, 2008). The Rho family members RhoA, Rac1 and Cdc42 are key regulators of the actin cytoskeleton and cell junction assembly (Heasman and Ridley, 2008). Recently, it has been shown that RhoA is required to maintain adherence junctions (AJs) in murine neuroepithelia (Herzog et al., 2011; Katayama et al., 2011). In the spinal cord, RhoA is required for AJs and for epithelial morphology (Herzog et al., 2011). In the fore- and midbrain, loss of RhoA results in the disruption of AJs, abnormal morphology and ectopic proliferation of neuroepithelia (Katayama et al., 2011).

Rho GTPases cycle between an active GTP-bound and an inactive GDP-bound state. Their activation is mediated by guanine nucleotide exchange factors (GEFs) (Rossman et al., 2005), which catalyze the exchange of GDP for GTP. Members of the Dbl-related RhoGEFs possess a dbl-homology (DH) domain that is responsible for their catalytic activity and a Pleckstrin homology (PH) domain, which is thought to mediate membrane localization and protein-protein interaction. *ArhGEF18* (*p114RhoGEF*) is a RhoA- and Rac1-specific GEF (Blomquist et al., 2000; Nagata and Inagaki, 2005; Niu et al., 2003). In cultured cells, *ArhGEF18* has been shown to regulate tight junction (TJ) assembly, cortical actin organization and cellular morphology (Nakajima and Tanoue, 2011; Terry et al., 2011). Its functional relevance for vertebrate development has not been addressed so far.

We used medaka fish (*Oryzias latipes*) as a vertebrate model system to identify genes that function in epithelial polarity in the context of the complex organism. The vertebrate retina with its simple organ architecture and available protocols to manipulate gene function is an excellent paradigm with which to study polarity of neuro-epithelia (Pujic and Malicki, 2001; Randlett et al., 2010). During embryogenesis, the retina develops from specified cells of the anterior neuroectoderm that evaginate from the forebrain as optic vesicles (Rembold et al., 2006b). These cells then form a pseudo-stratified single-layered neuro-epithelium and subsequently differentiate to give rise to the multilayered neural retina (Randlett et al., 2011).

In a chemical mutagenesis screen, we identified *ArhGEF18* as a gene essential for a-b polarity and morphology of retina and forebrain neuroepithelia. We show that *ArhGEF18* is essential for the maintenance of a-b polarity and proliferation control of the retinal neuroepithelium. Loss of *ArhGEF18* results in mislocalization of the apical determinant atypical protein kinase C (aPKC) and TJs, as well as disorganization of the actin cytoskeleton. Furthermore, cellular morphology and proliferation are perturbed. Our functional analysis indicates RhoA as the key target of ArhGEF18 and demonstrates that RhoA signals through Rock to control a-b polarity, tissue architecture and, by that, organ formation.

MATERIALS AND METHODS

Fish stocks

Medaka inbred lines Cab and Kaga were kept as described previously (Loosli et al., 2000). Embryos were staged according to Iwamatsu (Iwamatsu, 2004).

[1]Institute of Toxicology and Genetics, Karlsruhe Institute of Technology, Hermann von Helmholtz Platz 1, 76344 Eggenstein-Leopoldshafen, Germany. [2]Max Planck Institute for Heart and Lung Research, Ludwigstrasse 43, 61231 Bad Nauheim, Germany. [3]Developmental Biology, European Molecular Biology Laboratory, Meyerhofstrasse 1, 69117 Heidelberg, Germany. [4]Centre for Organismal Studies, University of Heidelberg, INF 230, 69120 Heidelberg, Germany. [5]Swiss Federal Institute of Intellectual Property, Stauffacherstrasse 65/59g, 3003 Bern, Switzerland.

*These authors contributed equally to this work
‡Author for correspondence (felix.loosli@kit.edu)

Accepted 15 April 2013

Molecular identification of *medeka*

med was mapped to chromosome 4 by bulk segregation analysis as described previously (Martinez-Morales et al., 2004). Marker MF01SSA020A05 (6/1006; 0.6cM) was the anchor point for a BAC walk using a panel of 885 mutant embryos (1770 meioses). Genomic sequence analysis revealed *ArhGEF18* between the two flanking markers with highest linkage. The *med* gene structure was determined by RACE (SMART-RACE, Clontech) and a full-length cDNA was cloned by RT-PCR (GenBank JN868075).

DNA constructs

The full coding sequence of *OlArhGEF18* was cloned with a N-terminal flag tag into pCS2. GFP was fused N-terminally using pEGFP-C1 and pCS2. OlArhGEF18ΔC was obtained by deleting 1480 bp (amino acids 563-1058). A 1360 bp in-frame deletion (amino acids 82-528) gave rise to OlArhGEF18ΔDH-PH. Human OlArhGEF18 (KIAA0521, Kazusa DNA Research Institute) was cloned into pCS2. T2A expression constructs were obtained by using a 54 bp T2A fragment to link N-terminal GFP with dominant-negative RhoA, Rac1 and Rock2. The constructs were then subcloned into a vector containing the zebrafish Hsp70 promoter and SV40 polyA. Heat-shock treatment was carried out at 37°C for 20 minutes. To label individual RPCs, a plasmid expressing GFP under the control of the *rx2* promoter was injected at the one-cell stage (Martinez-Morales et al., 2009).

RNA, DNA and MO injections

All injections were performed at the one-cell stage. Capped sense RNAs were synthesized (mMessage Machine, Ambion) and injected at 70-120 ng/μl. Expression constructs were injected at 15 ng/μl as described (Rembold et al., 2006a). *ArhGEF18* morpholinos were injected at 250-500 μm. For rescue analysis, all eggs from crosses of med^{23} and med^{34} carrier fish were injected, raised and analyzed at the appropriate stage.

Transplants

Cell transplantation at blastula stage was carried out as described previously (Rembold et al., 2006b).

BrdU labeling

BrdU solution (2 mM) was injected into the yolk. For labeling periods greater than 1 hour, 0.5 mM BrdU was injected. Embryos were fixed in 100 mM PIPES (pH 7) overnight at room temperature. Cryosections were treated with HCl 2 N for 45 minutes.

GTPase activation and stress fiber assay

The amount of activated cellular RhoA, Cdc42 and Rac1 were determined by precipitation with a fusion protein of GST and the Rho-binding domain of Rhotekin (GST-RBD) or the Cdc42/Rac1-binding domain of Pak1 (GST-Pak1), as described previously using HEK293 cells (Benard et al., 1999; Ren and Schwartz, 2000). Actin stress fibers of transfected NIH 3T3 cells were visualized by phalloidin labeling as described previously (Panizzi et al., 2007).

Immunohistochemistry

Immunohistochemistry was carried out as described previously (Martinez-Morales et al., 2009) with the following modifications: embryos were fixed in 100 mM PIPES (pH 7) overnight at room temperature. Blocking and antibody incubations were carried out in PBS, 1% DMSO, 1% BSA, 0.5% TritonX-100. Methylene Blue-Azure II stainings were carried out as described previously (Loosli et al., 2004).

Antibodies and molecular probes

The following primary antibodies and probes were used: α-phospho-histone H3 (1:200, Millipore 06-570); α-aPKC (1:500, Santa Cruz sc-216); α-ZO1 (1:400, Zymed 33-9100); zPr1 (1:100, ZIRC); α-GFP (1:500, Invitrogen A11122; JL-8 1:500, Clontech 632380); phalloidin Alexa-488/546 (1:10, Invitrogen A12379/A22283); and α-BrdU (1:750, Abd Serotec MCA2060GA). Primary antibodies were detected using secondary Alexa dye-conjugated antibodies (1:400, Molecular Probes).

Western blot analysis

Western blots were carried out as described previously (Martinez-Morales et al., 2009). The following primary antibodies were used: α-flag antibody (1:10,000, Sigma F3165-1MG); α- p114RhoGEF (1:500, Everest Biotech EB06163); α-RhoA (1:500, Cell Signaling 2117); α-Rac1 (1:1000, Millipore 05-389); α-ERK (1:10,000, Santa Cruz sc-94); and α-Rock2 (1:500, Anaspec 55431). Antibodies were visualized with secondary HRP-coupled antibodies (1:2000, Dako) using ECL (Amersham).

Statistical analysis

An algorithm, implemented in Matlab, identified and quantified the BrdU and pH3 expressions patterns using morphological filtering and boundary extraction. The classical one-way ANOVA test was used for the statistical comparison.

RESULTS

Morphology, proliferation and apicobasal polarity are affected in *medeka* mutant retinae

We used chemical mutagenesis in medaka fish to identify novel genes that function in epithelial polarity of the vertebrate retina (Furutani-Seiki et al., 2004; Loosli et al., 2004). We isolated two alleles of the mutation named *medeka*: med^{34} and med^{23}. The *med* phenotype is first detectable with the onset of retinal differentiation at stage 25 (2.5 dpf). The eyes are enlarged and pigmentation of the retinal pigment epithelium (RPE) is patchy (Fig. 1A,B). Histological sections showed that at 8 dpf retinal lamination is disrupted in the mutant and eye morphology is abnormal (Fig. 1C,D). Both alleles are recessive, larval-lethal mutations with complete penetrance (Table 1). Both were used for the phenotypic analysis and yielded indistinguishable results.

We examined whether altered cell proliferation causes enlarged mutant retinae. We used phospho-Histone H3 (pH3) as a marker for M-phase nuclei to determine the ratio of proliferating RPCs (Fig. 1E-G). At 2.5 dpf the ratio of pH3 positive to total nuclei was 1.4% in wild type, whereas in the mutant this ratio was increased to 2.3%. At 3 dpf the ratio was increased from 5.6% to 8.3%. At later stages (4 and 5 dpf), the increase in the mutant was much higher (2.5- and 9.3-fold, respectively; Fig. 1G; supplementary material Fig. S1A,B). The higher ratio of M-phase nuclei to total number of nuclei in mutant retinae indicates increased proliferation.

We then examined whether altered cell cycle progression results in the observed increase in cell proliferation. We used BrdU labeling at stage 27 (2.8 dpf) to determine the relative number of proliferating cells after different periods of incorporation (Fig. 1H-J; supplementary material Fig. S1C,D). We found no significant difference between the ratio of BrdU-positive cells to total cells in wild-type and mutant retinae after different periods of BrdU incorporation, suggesting that the fraction of cells entering S-phase similarly increases in mutant and wild type. Furthermore, BrdU and pH3 double-labeling experiments to analyze cell cycle progression from S- to M-phase at stage 27 revealed no significant difference between wild-type and mutant retinae (supplementary material Fig. S1G-I). In summary, this indicates that cell cycle progression is not altered in mutant RPCs.

We therefore examined whether reduced cell cycle exit of proliferating RPCs accounts for the increased proliferation in the mutant. To determine the relative number of cells that exited the cell cycle prior to 3 dpf and 4 dpf, respectively, we injected BrdU at these time points and analyzed the incorporation after 12 hours of development. The ratio of BrdU-negative to DAPI-positive cells was determined, giving the relative number of cells that exited the cell cycle prior to the BrdU injection (Luo et al., 2012). In wild type, 43% and 48% cells were BrdU negative at 3 and 4 dpf, respectively, whereas in the mutant this ratio was reduced to 2.4% and 6%, respectively (Fig. 1K-M; supplementary material Fig. S1E,F). Ectopic BrdU-positive nuclei were localized in the central mutant

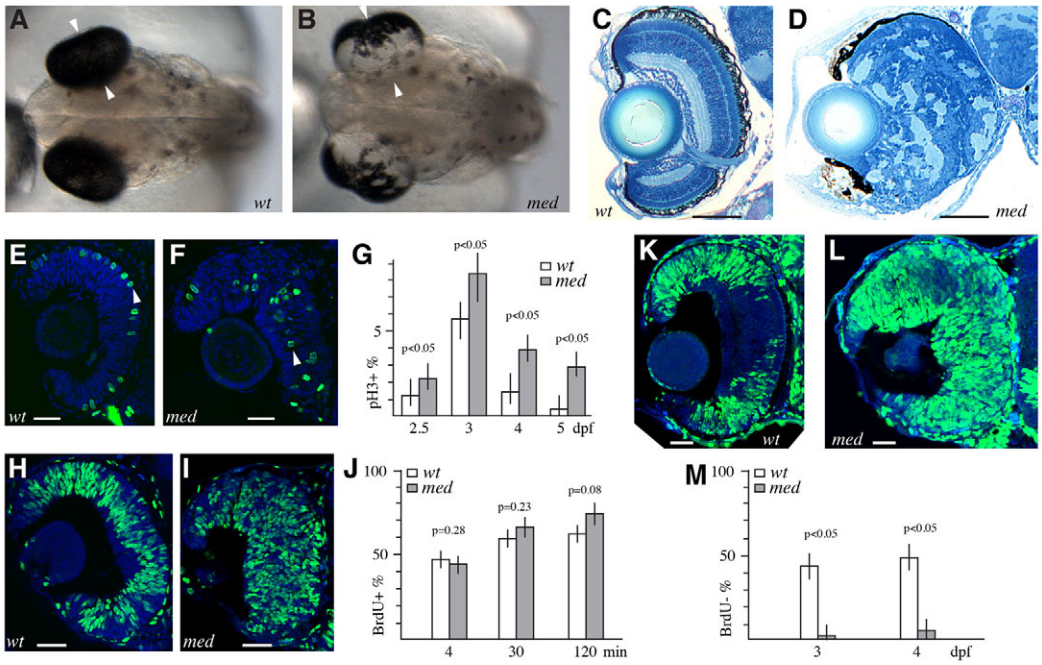

Fig. 1. *med* affects retinal morphology and proliferation. (**A**,**B**) Dorsal view of 4 dpf embryos; anterior towards the right. The mutant (B) is enlarged (arrowheads) and RPE pigmentation is patchy. (**C**,**D**) 8 dpf histological transverse sections shows that the mutant retina (D) is thicker with abnormal morphology and absent lamination. (**E**,**F**) Wild-type M-phase nuclei (α-pH3, green) at stage 25 are apically localized (E, arrowhead); in the mutant they are often more basally positioned (F, arrowhead). (**G**) Ratio of pH3-positive to total nuclei in wild-type and mutant retinae at 2.5, 3, 4 and 5 dpf. In the mutant, the ratio is significantly increased at all stages. (**H**,**I**) BrdU labeling (green) of wild-type and mutant retinae at 2.8 dpf. Both wild type and mutant show ~45% positive nuclei after 4 minutes BrdU incorporation. (**J**) Ratio of BrdU-positive to total nuclei after 4, 30 and 120 minutes BrdU incorporation with no significant differences between wild-type and mutant. (**K**,**L**) 12 hour BrdU labeling at 3 dpf. The central region of the wild-type retina is unlabeled, whereas the mutant is ubiquitously labeled. (**M**) Ratio of BrdU-negative to total nuclei after a 12-hour incorporation in wild type and mutant at 3 and 4 dpf. A significant strong decrease is observed in mutant retinae. (E,F,H,I,K,L) Confocal transverse sections, DAPI-stained nuclei (blue). Scale bars: 100 μm in C,D; 25 μm in E,F,H,I,K,L.

retina, where, in the wild type, differentiating cells reside that exited the cell cycle. This indicates that cell cycle exit by neurogenic divisions is strongly reduced in mutant RPGs at 3 and 4 dpf. This is consistent with the observed increase of the fraction of proliferating pH3-positive RPCs in the mutant from 2.5 to 5 dpf (Fig. 1G). Consistent with the location of ectopic BrdU-positive nuclei, these ectopic pH3-positive RPCs were mostly in the central region of the retina at 3-5 dpf (supplementary material Fig S1A,B and data not shown). Furthermore, analysis of cell cycle exit at stage 27 (2.8 dpf) using ath5 as a marker for neurogenic divisions (Del Bene et al., 2007; Yamaguchi et al., 2010) provided further evidence that cell cycle exit is significantly reduced in *med* mutant retinae (supplementary material Fig. S1J-L). We therefore conclude that cell cycle progression is normal in mutant RPCs, whereas cell cycle exit is severely reduced, leading to the observed increase in RPC proliferation.

Similar phenotypes in the developing retina were observed in zebrafish mutants affected in a-b polarity (Jensen and Westerfield,

Table 1. Phenotypic rescue by ArhGEF18 RNA injection

RNA	Allele	*n*	Wild type	Severe mutant	Medium mutant	Weak mutant
ArhGEF18	34	104	80	0	0	24 (23%)
	23	130	101	0	1 (1%)	28 (22%)
GFP-ArhGEF18	34	120	93	0	0	27 (23%)
	23	108	81	0	0	27 (25%)
hArhGEF18	34	134	95	0	5 (5%)	34 (25%)
	23	90	68	0	3 (3%)	19 (21%)
ArhGEF18ΔC	34	104	76	24 (23%)	2 (2%)	0
	23	203	156	47 (23%)	0	0
ArhGEF18ΔDH-PH	34	161	120	41 (25%)	0	0
	23	163	117	46 (28%)	0	0
GFP	34	132	102	30 (23%)	0	0
	23	85	69	16 (19%)	0	0
Uninjected	34	99	75	24 (24%)	0	0
	23	134	104	30 (22%)	0	0

The total number of injected embryos (*n*) and number of embryos in the respective phenotypic classes are indicated. Injection of full-length medaka (ArhGEF18) and human *ArhGEF18* (hArhGEF18) rescues the mutant phenotype. Deletion of the C-terminal region (ArhGEF18ΔC) and the DH-PH domains (ArhGEF18ΔDH-PH) abolishes rescue activity. GFP-tagged medaka *ArhGEF18* (GFP-ArhGEF18) rescues with the same efficiency as wild-type ArhGEF18. Control-injected embryos (GFP) are not rescued.

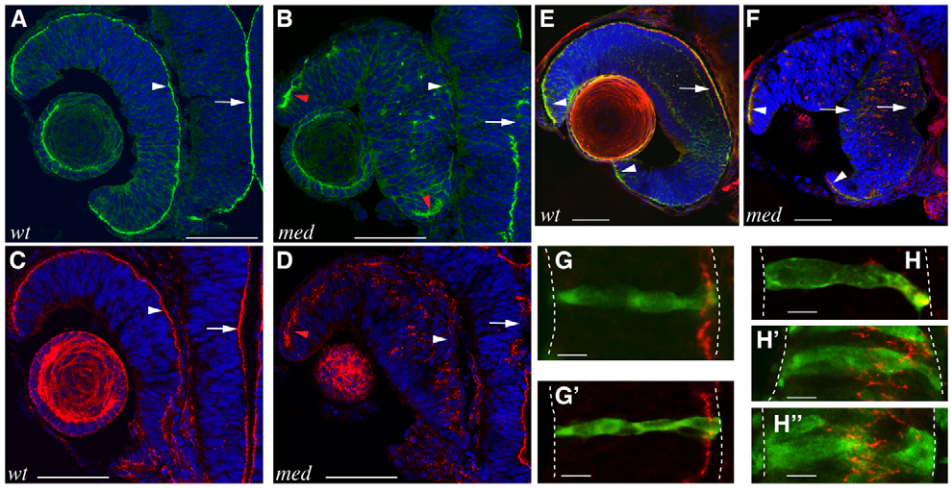

Fig. 2. *med* perturbs apicobasal polarity. (**A-D**) Localization of aPKC (green; A,B) and ZO1 (red; C,D) in wild type (A,C) and mutant (B,D) at stage 25. Apical localization of aPKC and ZO1 in the mutant retina is compromised with mislocalized foci (B,D, white arrowheads). CMZ (red arrowheads) and brain are less severely affected (B,D, arrows). (**E**,**F**) aPKC (green) and ZO1 (red) localization in wild-type (E) and mutant (F) retinae at 4 dpf. (F) aPKC and ZO1 apical localization is normal in the mutant CMZ (arrowheads), with aPKC apical to and partially overlapping with ZO1. In the central mutant retina, aPKC is not detectable and ZO1 is mislocalized (arrows). (**G-H″**) Localization of ZO1 (red) in single wild-type (G,G′) and mutant (H-H″) GFP-labeled RPCs (green) at early stage 25 (G,H), late stage 25 (H′) and early stage 26 (G′,H″). (G-H″) Apical localization of ZO1 gradually deteriorates in mutant RPCs and the initially columnar epithelial cell morphology is lost at early stage 26 (H-H″). (A-H″) Confocal transversal sections. (A-F) DAPI-stained nuclei (blue). (G-H″) Epithelial a-b extent is indicated by broken lines. Scale bars: 50 μm in A-F; 7.5 μm in G-H″ .

2004; Malicki, 2004; Omori and Malicki, 2006). We therefore examined whether *med* perturbs a-b polarity. Atypical protein kinase C (aPKC) is a key regulator of a-b polarity with apical localization (Horne-Badovinac et al., 2001). In the wild-type retina and forebrain, aPKC is apically localized at stage 25, whereas in the mutant retina this localization is almost completely abolished (Fig. 2A,B, arrowheads). In the forebrain, aPKC localization is less severely affected (Fig. 2A,B, arrows). Thus, a-b polarity is severely perturbed by the *med* mutation.

The TJ associated protein ZO1 (Hartsock and Nelson, 2008) is apically localized in the wild-type retina and forebrain at stage 25 (Fig. 2C). In the mutant retina, TJs are displaced (Fig. 2D, arrowhead) and in the forebrain the apical TJ belt shows gaps (Fig. 2D, arrow). Thus, in addition to a-b polarity the location of TJ is also perturbed.

In teleosts, retinal differentiation proceeds in a wave-like fashion from the central retina towards the periphery. Thus, at 4 dpf the central retina contains differentiating postmitotic cells, whereas RPCs in the ciliary marginal zone are still proliferating (supplementary material Fig. S1A,E). We noticed that at this stage in mutant CMZ both aPKC and TJs (ZO1) are apically localized similar to the wild-type situation (Fig. 2E,F, arrowheads), whereas in the mutant central retina aPKC is not detectable and TJs are delocalized (Fig. 2F, arrows). Apical localization of aPKC and ZO1 are also less affected in CMZ at stage 25 (Fig. 2B,D, red arrowheads). As a-b polarity and TJ localization are less affected in proliferating mutant RPCs of the CMZ, we conclude that *med* affects the maintenance of a-b polarity and TJ localization rather than the initiation.

To examine the morphology and organization of RPCs, we labeled individual cells by expressing GFP under the control of the RPC-specific *rx2* promoter (Martinez-Morales et al., 2009). During stage 25 and early stage 26, wild-type RPCs have an elongated columnar shape and span the entire layer of the epithelium (Randlett et al., 2011) (Fig. 2G,G′). ZO1 is localized apically in an ordered line of foci just below the apex of the cell. At early stage 25, mutant RPCs also span the entire layer of the epithelium with an elongated and columnar morphology similar to the wild type, albeit often slightly bent (Fig. 2H). However, ZO1 localization is scattered over a wide range along the a-b axis. At late stage 25, mutant RPCs retain an elongated morphology in which ZO1 is further delocalized and often is found in elongated ribbons (Fig. 2H′). At early stage 26, mutant RPCs have lost their elongated morphology and ZO1 is scattered over a broad region in the middle of the epithelial layer (Fig. 2H″). Thus, initially the overall morphologically of mutant RPCs is normal with severely compromised a-b polarity. Subsequently, the morphology deteriorates, resulting in a disorganized cellular arrangement. We therefore conclude that the mutation initially affects a-b polarity, which as a consequence results in abnormal morphology of the cells and the epithelial organization of the entire tissue.

The *medeka* gene encodes ArhGEF18

We positionally cloned the causative gene by bulk segregation analysis (Martinez-Morales et al., 2004) and a subsequent BAC walk. The region with highest linkage contains a single gene, *ArhGEF18*. The *ArhGEF18* locus spans about 20 kb and comprises 20 exons (Fig. 3A). The open reading frame of 3177 bp encodes 1058 amino acids (119 kDa) with an N-terminal DH domain of 196 amino acids, followed by a PH domain of 52 amino acids (Fig. 3B; supplementary material Fig. S2). Both the DH and PH domains are highly conserved within vertebrate homologues, ranging from 60-65% and 67-71%, respectively (supplementary material Fig. S2). The C-terminal part of 604 amino acids is less well conserved (40%, supplementary material Fig. S2). *ArhGEF18* RNA is expressed ubiquitously at neurula and early organogenesis stages (Fig. 3C,D). By western blot analysis using an antibody raised against the human *ArhGEF18* protein (Terry et al., 2011), we detected a protein of the expected size (~120 kDa) in extracts of whole wild-type embryos from 1 to 4 dpf (Fig. 3E).

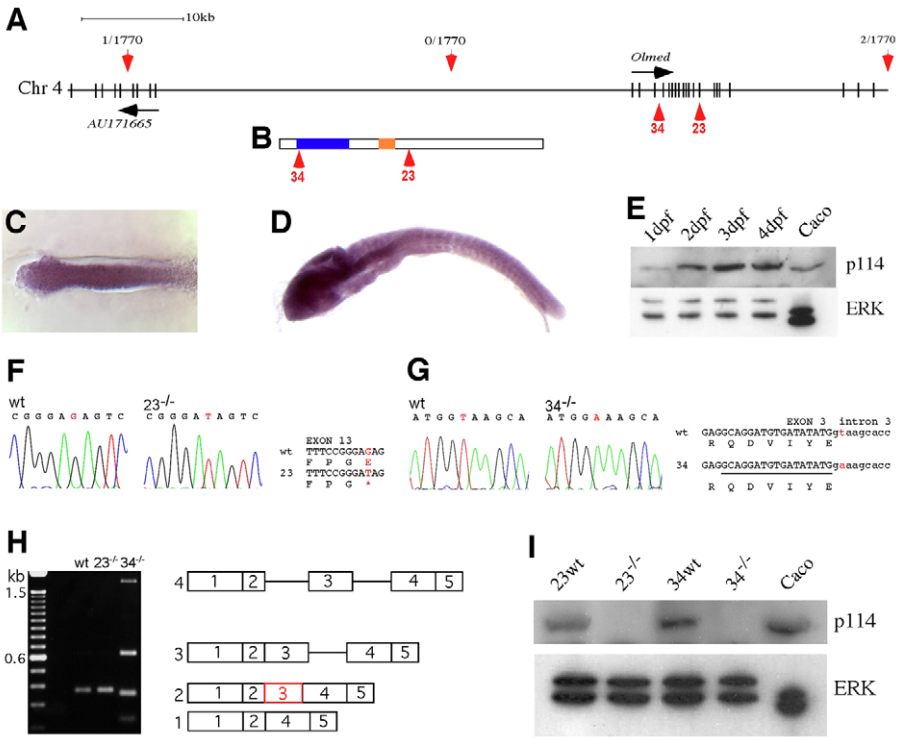

Fig. 3. *med* locus and expression analysis. (**A**) Physical map of the *med* locus on chromosome 4. The position of mapping markers is indicated (red arrows), direction of transcription (black arrows) and position of the mutations (red arrowheads) are shown. (**B**) Structure of the predicted Med protein. The DH (blue) and PH domain (orange), and positions of the mutations (red arrowheads) are indicated. (**C**,**D**) Whole-mount *in situ* hybridization analysis reveals ubiquitous expression of *ArhGEF18* mRNA at neurula stage (C) and early organogenesis stage (D). (**E**) Western blot analysis of ArhGEF18 expression (p114) (120 kDa) in embryos and human protein (114 kDa) in Caco cells as a control. Weak expression at 1 dpf subsequently increases. ERK is a loading control. (**F**) Genomic sequence of exon 13 in wild-type and mutant allele 23-3-7. The nonsense mutation G→T (red) is shown. (**G**) Exon-intron junction 3 in wild-type and mutant allele 34-10-1 with an intronic mutation in the 5′ splice site (red). The 17 bp skipped by mutant splicing (H: splice variant 2) are underlined. (**H**) RT-PCR analysis of *med* transcripts in wild type, alleles 23-3-7 and mutant splice variants of 34-10-1. (**I**) Full-length ArhGEF18 protein (p114) is not detectable by western blot analysis in $23^{-/-}$ and $34^{-/-}$ embryos. Human ArhGEF18 protein in Caco cells is shown as a control. ERK is a loading control.

Whole-mount *in situ* hybridization analysis revealed expression of *ArhGEF18* both in med^{23} and med^{34} mutant embryos (data not shown). Sequence analysis uncovered a nonsense point mutation in exon 13 of the med^{23} allele that results in a truncation of 458 C-terminal amino acids (Fig. 3B,F). In the med^{34} allele, a point mutation in intron 3 leads to aberrant splicing, giving rise to four mutant transcripts (Fig. 3B,G,H). In three of those, frame shifts due to aberrant splicing result in a deletion of both DH and PH domains and the entire C-terminal region. As the DH and PD domains are required for GTPase activation (see below), these truncations most likely result in a loss of function. The fourth low abundant mutant transcript encodes a protein with an in-frame 45 amino acid deletion in the DH domain. Western blot of whole embryo extracts probed with an antibody raised against the C terminus showed that full-length *ArhGEF18* protein is present at stage 25 in the wild-type but not in med^{23} and med^{34} mutants (Fig. 3I). Thus, the low abundant in-frame deletion transcript of med^{34} does not give rise to detectable protein levels. Our functional analysis showed that a C-terminal truncation of ArhGEF18 as in med^{23} results in a complete loss of function (see below). We therefore conclude that both alleles are amorphic or at least strongly hypomorphic.

To demonstrate that loss-of-function mutations of *ArhGEF18* are responsible for the observed phenotypes in both *med* alleles, we performed morpholino-based loss-of-function, as well as rescue experiments. We designed splicing morpholino oligonucleotides (MO) to disrupt *ArhGEF18* function in wild-type embryos. MO-injection resulted in phenocopies of the *med* mutation, including abnormal pigmentation and morphology, ectopic proliferation and aPKC mislocalization (supplementary material Fig. S3A-H), providing further evidence that *ArhGEF18* is the gene mutated in the *med* alleles. To test whether restoring wild-type protein in mutant embryos can rescue the *med* phenotype, we injected RNA encoding full-length ArhGEF18 at the one-cell stage into embryos from med^{23}- and med^{34}-carrier intercrosses. Phenotypical analysis of injected embryos showed that both pigmentation and eye morphology were rescued in mutant embryos at 3 dpf (Fig. 4A-D; Table 1). Moreover, at 7 dpf, injected mutant embryos exhibited a partial rescue of retinal lamination and localization of photoreceptors (Fig. 4E-G). In addition, full-length human ArhGEF18 (hArhGEF18) rescued the *med* mutation to the same degree with comparable efficiency (Fig. 4A; Table 1). This suggests that *ArhGEF18* function in neuro-epithelia is conserved throughout vertebrates. Embryos injected with GFP RNA as negative control showed no rescue of either morphology or retinal lamination (Fig. 4D,G; Table 1). Injection of RNA encoding ArhGEF18 with a C-terminal deletion (amino acids 563-1058, ArhGEF18ΔC), similar to the predicted truncated protein of allele med^{23} (600-1058), did not rescue the mutant phenotype of either med^{23} or med^{34} mutant embryos (Fig. 4A; Table 1). In addition, deletion of the DH and PH domains (ArhGEF18ΔDH-PH) abolished rescue activity completely

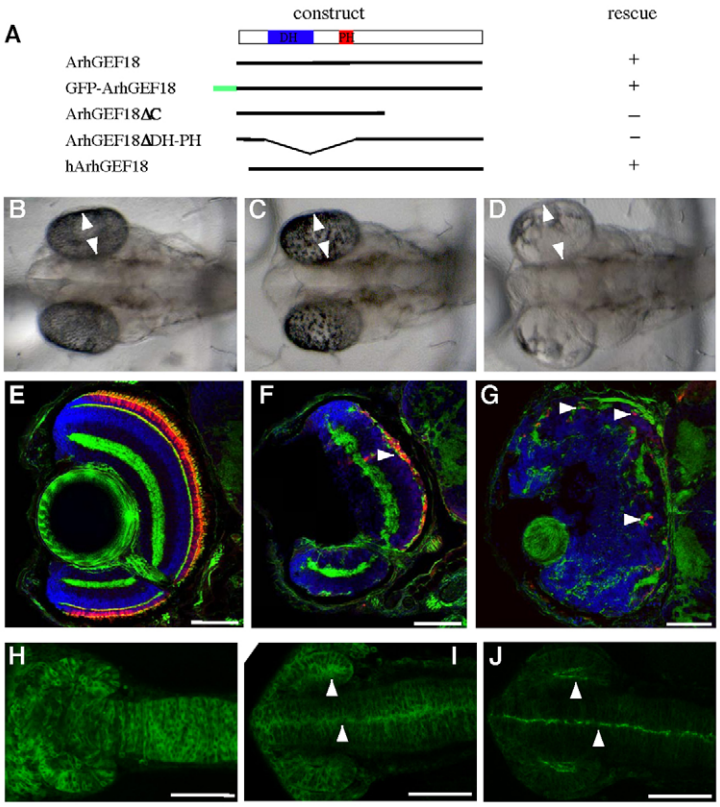

Fig. 4. *ArhGEF18* RNA injection rescues the mutant phenotype. (**A**) Full-length medaka (ArhGEF18), GFP-tagged (GFP-ArhGEF18), deletion variants (ArhGEF18ΔC, ArhGEF18ΔDH-PH) and human (hArhGEF18) cDNA used for RNA injections are shown. The rescue activity is indicated. The positions of the DH (blue) and PH (red) domains is shown. (**B-D**) Dorsal views of uninjected wild type (B), *ArhGEF18* mRNA-injected mutant (C) and *GFP* mRNA control-injected mutant (D) at 3 dpf. Eye morphology (arrowheads) and pigmentation is rescued (C). (**E-G**) Confocal transverse sections showing cone photoreceptors labeled by Zpr1 immunoreactivity (red) and actin by phalloidin staining (green) in 7 dpf uninjected wild type (E), *OlArhGEF18* mRNA-injected (F) and control-injected mutant (G). Retinal lamination and localization of photoreceptors (arrowheads) are rescued (F). (**H-J**) Coronal confocal sections of embryos injected with *GFP-OlArhGEF18* mRNA (H,I) and *Par3-GFP* RNA (J). Ubiquitous cytoplasmic distribution of GFP-ArhGEF18 at stage 18 (H) and apically enriched graded localization (arrowheads) at stage 21 (I), when Par3-GFP is apically localized (J, arrowheads). (E-G) DAPI-stained nuclei (blue). Scale bars: 75 μm in E-G; 100 μm in H-J.

(Fig. 4A; Table 1). Thus, the DH-PH domains, as well as the C-terminal region, are essential for ArhGEF18 function. In summary, the map position, sequence analysis, MO-phenocopy and RNA-rescue data show that the identified mutations in *ArhGEF18* alone cause the *med* phenotype, thus excluding second site modifiers.

To analyze the subcellular localization of ArhGEF18 in embryos, we N-terminally fused GFP to ArhGEF18. Injection of RNA encoding GFP-ArhGEF18 rescues mutant embryos with comparable efficiency to untagged ArhGEF18 (Fig. 4A, Table 1). This indicates that the *GFP-ArhGEF18* fusion protein is fully functional. We found that GFP-ArhGEF18 is homogenously distributed in the cytoplasm at stage 18 upon RNA injection (Fig. 4H). Eight hours later at stage 21, GFP-ArhGEF18 is apically enriched with low levels in the cytoplasm (Fig. 4I). We observed in medaka a gradual apical localization of Par3-GFP during this period (data not shown and Fig. 4J), similar to the gradual Par3 localization during zebrafish development (Tawk et al., 2007). Therefore ArhGEf18 becomes apically enriched alongside known regulators of a-b polarity, in line with a function of *ArhGEF18* in epithelial polarity.

Medaka ArhGEF18 activates RhoA and Rac1, but not Cdc42

The presence of a highly conserved DH domain strongly suggested a function for *ArhGEF18* as activator of small GTPases. To determine the specificity, we used cell culture based activation assays. It has been shown that human ArhGEF18 activates RhoA and Rac1 (Blomquist et al., 2000; Nagata and Inagaki, 2005; Niu et al., 2003; Terry et al., 2011), suggesting a similar specificity for medaka ArhGEF18, as human ArhGEF18 rescues the *med* phenotype. To test this hypothesis, we used the Rho-binding domain (RBD) of rhotekin to affinity precipitate activated RhoA and the Rac1/Cdc42-binding domain of PAK to affinity precipitate activated Rac1 and Cdc42. In HEK293 cells transfected with plasmids encoding either full-length medaka ArhGEF18 or only the DH-PH domains, we found a robust activation of both RhoA and Rac1 but not of Cdc42 (Fig. 5A-C). Deletion of the DH-PH domains (ArhGEF18ΔDH-PH) completely abolished the activation of RhoA and Rac1. Thus, medaka ArhGEF18 can activate both RhoA and Rac1, and therefore shares the specificity with the human homologue. The finding that both activation of RhoA and Rac1 GTPases, as well as rescue of the mutant phenotype, require the DH-PH domains, confirms GTPase activation as a key function of ArhGEF18 in regulating a-b polarity.

Activation of RhoA induces the formation of actin stress fibers (Popoff and Geny, 2009) and it has been shown that human ArhGEF18 can induces stress fibers in J82, NIH3T3 and COS7 cells (Blomquist et al., 2000; Nagata and Inagaki, 2005; Niu et al., 2003). We therefore tested the ability of medaka ArhGEF18 to induce stress fibers in cultured NIH3T3 cells. Stress fibers were formed by cells expressing full-length ArhGEF18 and, as a positive control, activated RhoA (Fig. 5D). This provides further evidence that ArhGEF18 is an activator of RhoA.

ArhGEF18 activity is required in the neural retina and regulates cortical actin and TJ localization

To address the cell autonomy of *med* function, we analyzed chimeras upon blastomere transplantation of biotin-labeled cells. In control transplantations, wild-type cells gave rise to clones of variable size at 3.5 dpf, where cells contributed normally to the host retina (Fig. 6D). Single cell mutant clones in wild-type host tissue showed wild-type morphology and normal apical localization of aPKC, indicating that the *med* mutation acts cell non-autonomously in these single cells (Fig. 6A,B, arrows). However, in larger mutant clones, cells were morphologically abnormal and apical aPKC was absent or strongly reduced (Fig. 6A,B, arrowheads), indicating cell

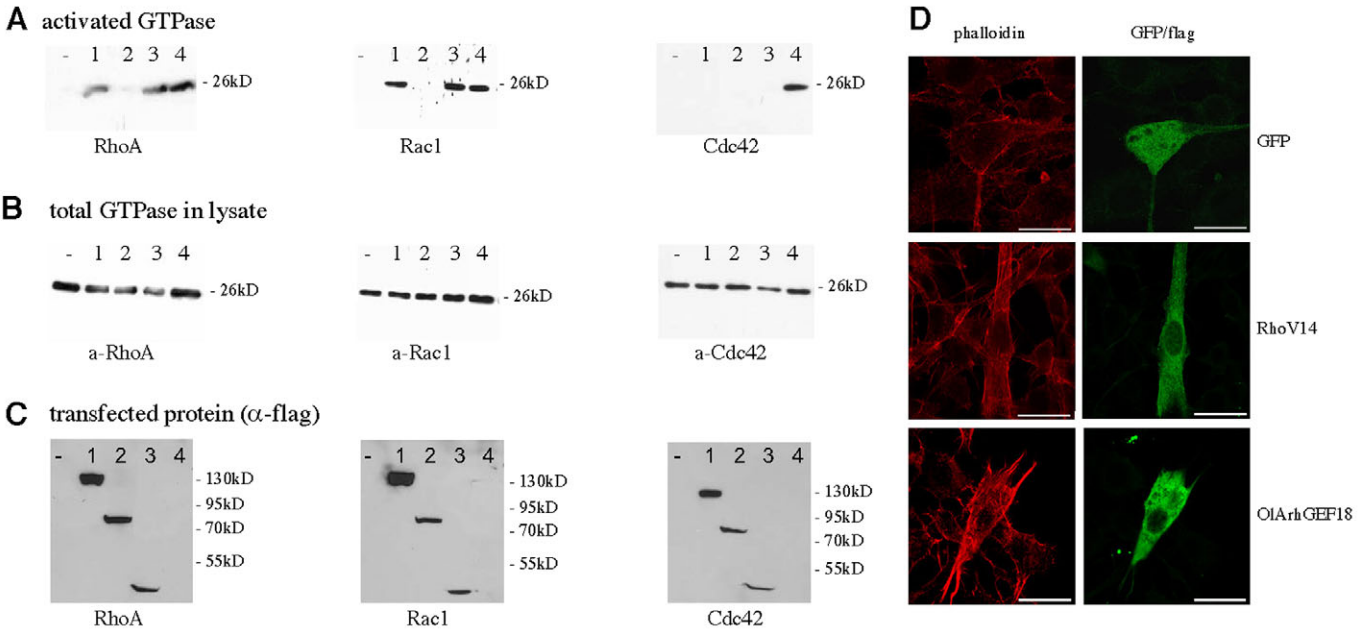

Fig. 5. ArhGEF18 activates RhoA and Rac1, but not Cdc42, and induces stress fibers. (**A-C**) GTPase activation by AhrGEF18 in HEK 293 cells. Lanes are labeled as follows: -, pCS2 control; 1, pCS ArhGEF18; 2, pCS ArhGEF18ΔDH-PH; 3, pCS DH-PH; 4, positive controls, pCMV RhoV14, pCMV Rac L61 and pCMV Cdc42 L61. (A) Expression of full-length medaka ArhGEF18 or only DH-PH domains activates RhoA and Rac1 but not Cdc42. Deletion of DH and PH domains abolishes RhoA and Rac1 activation, respectively. (B) Total amount of RhoA (α-RhoA), Rac1 (α-Rac1) and Cdc42 (α-Cdc42) in cell lysates. (C) Total amount of flag-tagged ArhGEF18, ArhGEF18ΔDH-PH and DH-PH proteins in cell lysates. (**D**) Actin stress fiber induction in NIH 3T3 cells transfected with pCMV ArhGEF18 and pCMV GFP-RhoAV14 as positive control; pCMV GFP is a negative control. Scale bars: 25 μm.

autonomy. Wild-type cells transplanted to mutant hosts never gave rise to clones contributing to the mutant retina, but formed small clones outside of the mutant host retina (data not shown). The genotype of RPE cells did not affect the phenotype of abutting neuroretinal cells. Wild-type RPE cells could not rescue the mutant phenotype of an abutting mutant retinal clone (Fig. 6A,B, arrowheads). Furthermore, mutant RPE cells did not affect wild-type cells of the underlying neuroretina (Fig. 6C, arrowhead). Thus, ArhGEF18 activity is required in the neural retina.

As ArhGEF18 induces actin stress fibers in cell culture, we analyzed how ArhGEF18 regulates the actin cytoskeleton of RPCs. We found that in wild-type RPCs at stage 26, cortical actin is concentrated in basal and apical bundles. Apical bundles are arranged in a string-of-beads fashion (Fig. 6E). TJ-associated ZO1 colocalizes apically with these actin foci (Fig. 6E, arrow). In mutant RPCs, apical actin localization in bundles is irregular with large gaps and colocalization with ZO1 is frequently lost (Fig. 6F, arrow). Therefore, ArhGEF18 is required for both cortical actin localization and also for the association of apical actin bundles with TJs. We observed that actin bundle localization and colocalization with ZO1 is less affected in RPCs of the CMZ at the distal retina, providing evidence that ArhGEF18 function is required for the maintenance of cortical actin localization rather than its initiation (Fig. 6E, red arrowhead). Consistent with our findings, in human intestinal and corneal epithelial cell lines ArhGEF18 is also required for TJ formation and actin localization (Terry et al., 2011).

RhoA/Rock but not Rac1 regulate a-b polarity, cell morphology and TJ localization in RPCs

Several lines of evidence suggest that ArhGEF18 activates Rho in the medaka embryo. Medaka ArhGEF18 activates RhoA in HEK293 cells and induces stress fibers (Fig. 5A,D), a process that requires RhoA activation (Popoff and Geny, 2009). Consistently, we found that ArhGEF18 regulates cortical actin localization in RPCs (Fig. 6E,F). Finally, human ArhGEF18, which can rescue the *med* mutant phenotype, regulates cell morphology and cortical actin in a RhoA-dependent manner in epithelial cell lines (Terry et al., 2011). We therefore tested the hypothesis that ArhGEF18 activates RhoA to regulate a-b polarity, actin cytoskeleton and cell morphology of the retinal neuroepithelium.

Medaka RhoA and Rac1 homologues are highly conserved and expressed in the developing central nervous system during early embryogenesis, consistent with a role in cell polarity and epithelial morphogenesis (supplementary material Fig. S4A,B). To test whether they function in these processes, we interfered with RhoA and Rac1 signaling by expressing dominant-negative variants (GFP-T2A-dnRhoA, GFP-T2A-dnRac1). Rho-kinase2 (Rock2), a direct RhoA effector is a key regulator of the actin cytoskeleton and adhesion complexes (Riento and Ridley, 2003). We therefore used a dominant-negative Rock2 variant (Marlow et al., 2002) to test whether RhoA-Rock2 signaling regulates a-b polarity in addition to the actin cytoskeleton.

Interfering with RhoA signaling during early embryogenesis severely perturbs gastrulation (Marlow et al., 2002; Matsui et al., 2005). Thus, we used the zebrafish hsp70 promoter (Blechinger et al., 2002) for a temporal control of expression in combination with T2A-based constructs (Szymczak et al., 2004) that allow GFP-tagging of expressing cells (supplementary material Fig. S5).

We injected GFP-T2A-dnRhoA, GFP-T2A-dnRock2 and GFP-T2A-dnRac1 plasmid DNA at the one cell stage and embryos were heat-shocked at stage 23, 6 hours before the *med* phenotype is detectable. At this stage, a-b polarity is established in the embryonic CNS (Fig. 4J). At stage 25, injected embryos expressing GFP in the retina were analyzed by antibody staining. The morphology of

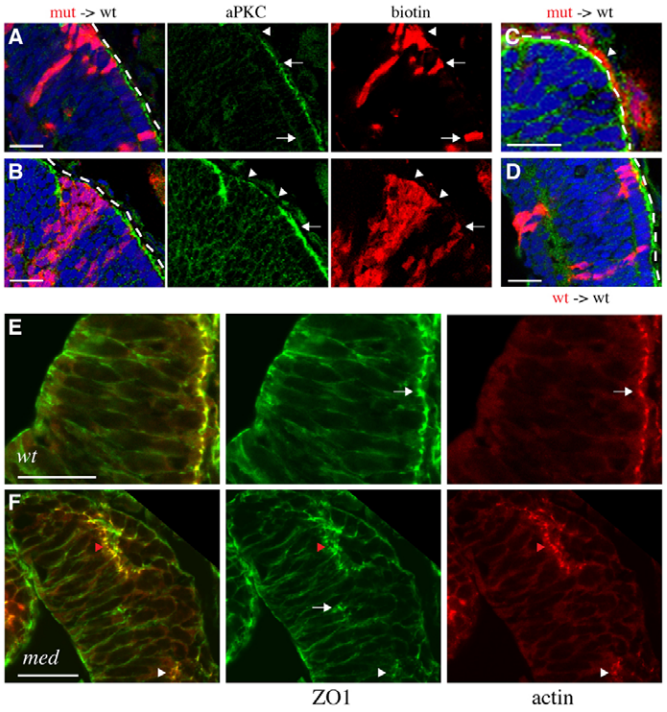

Fig. 6. Cell autonomy of ArhGEF18 function and its role for cortical actin and tight junction localization. (**A-D**) Mosaic analysis of biotin-labeled transplanted cells (red) at 3.5 dpf. Dashed line indicates border between RPE and neural retina. (A,B) Isolated single mutant cell clones have apical aPKC (green) localization and normal cell morphology (A,B, arrows). In large mutant clones, apical aPKC is absent and cell morphology is abnormal (A,B, arrowheads). Wild-type RPE cells cannot rescue abutting neuroretina (A,B arrowheads). (C) Mutant RPE cells do not affect a-b polarity of adjacent wild-type cells (arrowhead). (D) Transplanted control wild-type cells contribute normally to all nuclear layers. (**E**,**F**) TJ (ZO1, red) and actin (phalloidin, green) localization at stage 26. (E) Wild-type cortical actin is enriched apically and basally; tight junctions colocalize with apical actin foci (arrow). (F) Mutant apical and basal actin localization and colocalization with TJs is perturbed (arrow). The CMZ is less affected (red arrowheads) than the proximal retina (white arrowheads). (A-E) Confocal transverse section. (A-D) DAPI-stained nuclei (blue). Scale bars: 25 μm.

RPCs expressing either dnRhoA or dnRock2, as visualized by GFP, was often rounded, whereas control RPCs expressing only GFP exhibited the normal elongated morphology (Fig. 7A-C). Concomitant with cell morphology, aPKC and ZO1 localization was also perturbed, leading to mislocalization or complete absence of these proteins (Fig. 7B,C, arrowheads). Expression of dnRac1 did not affect RPC morphology, aPKC and ZO1 localization (Fig. 7D). Thus, RhoA is required to maintain both a-b polarity (aPKC) and localization of TJ (ZO1), and also regulates cell morphology in RPCs. As the effects of dnRhoA and dnRock2 were comparable, our findings indicate that RhoA signals mainly through Rock2 in these processes.

We then analyzed the effects on cortical actin localization. In control injected embryos expressing only GFP, cortical actin showed wild-type localization with basal and apical actin bundles (supplementary material Fig. S6A). In RPCs expressing either dnRhoA or dnRock2, apical actin bundles were mislocalized or absent, whereas basal actin was less severely affected (supplementary material Fig. S6B,C, arrowheads). Expression of dnRac1 did not affect the actin cytoskeleton (supplementary material Fig. S6D). Thus, blocking RhoA or Rock2 perturbs cortical actin localization similar to the situation in *med* mutant RPCs. This supports the hypothesis that ArhGEF18 activates RhoA-Rock2 signaling to also regulate the actin cytoskeleton.

In *med* mutant RPCs M-phase nuclei are often basally mislocalized. In RPCs expressing either dnRhoA or dnRock2, we found that pH3-positive M-phase nuclei were basally displaced (supplementary material Fig. S6B,C, arrowheads). In RPCs expressing only GFP or dnRac1, M-phase nuclei were at the apical surface or displaced less than 1 nuclear diameter basally (supplementary material Fig. S6A,D, arrowheads). Thus, RhoA-Rock2 signaling is crucial for proper positioning of M-phase nuclei.

DISCUSSION

We used the teleost medaka to address the function of *ArhGEF18* in the developing vertebrate embryo. We found that in the vertebrate neuroepithelium *ArhGEF18* regulates the organization of the actin cytoskeleton and localization of TJs. In addition we uncovered novel roles for *ArhGEF18*, namely controling apicobasal polarity and proliferation. In vertebrate cell culture systems, *ArhGEF18* has been identified as an important regulator of RhoA (Nakajima and Tanoue, 2011; Terry et al., 2011). Our functional analysis in the embryo shows that ArhGEF18 activates RhoA-Rock2 signaling to regulate epithelial apico-basal polarity. Thus, our analysis of *ArhGEF18* function in the context of vertebrate embryonic development provides novel insights into the function of both *ArhGEF18* and also RhoA.

RhoA is mainly implicated in the regulation of the actin cytoskeleton and associated AJ (Samarin and Nusrat, 2009). The conditional knockout of RhoA in the mouse embryonic CNS perturbs neuroepithelial organization as well as AJ maintenance. In the spinal cord, RhoA knockout resulted in reduced proliferation and premature cell cycle exit of progenitor cells (Herzog et al., 2011). This is in contrast to RhoA knockout in the fore- and midbrain, resulting in increased proliferation and decreased cell cycle exit (Katayama et al., 2011), similar to *med* mutant RPCs. Furthermore, in the spinal cord the actin regulator mDia has been identified as RhoA effector that regulates epithelial integrity (Herzog et al., 2011), whereas our work indicates Rock2 as effector of Rho signaling in the retina. This indicates that the role of RhoA signaling in the vertebrate CNS is cell type dependent and likely to involve different activators and effectors. Thus, animal models will be instrumental in deciphering the complexity of vertebrate RhoA signaling.

Starting at stage 26, wild-type RPCs undergo neurogenic divisions and exit the cell cycle (Del Bene et al., 2007), resulting in a decrease of proliferating cells in the neurogenic region in the central retina. Cell cycle exit of *med* mutant RPCs is decreased and, as a consequence, the relative number of proliferating RPCs is severely increased. In addition, mutations in *Ncadherin* and *Pals1* result in decreased neurogenic divisions of RPCs in the zebrafish retina, suggesting that apico-basal polarity regulates the balance between proliferative and neurogenic divisions (Yamaguchi et al., 2010). It has been hypothesized that segregation of cellular determinants and nuclear position along the a-b axis during cell divisions are crucial for this process. Recently, the Hippo tumor suppressor pathway emerged as a key regulator of growth and proliferation (Bao et al., 2011; Halder and Johnson, 2011). Upstream regulators of this pathway also include the polarity determinant Crumbs, which provides a possible molecular link between a-b polarity and growth control by Hippo signaling. The actin cytoskeleton also regulates the Hippo pathway. Induction of extra F-

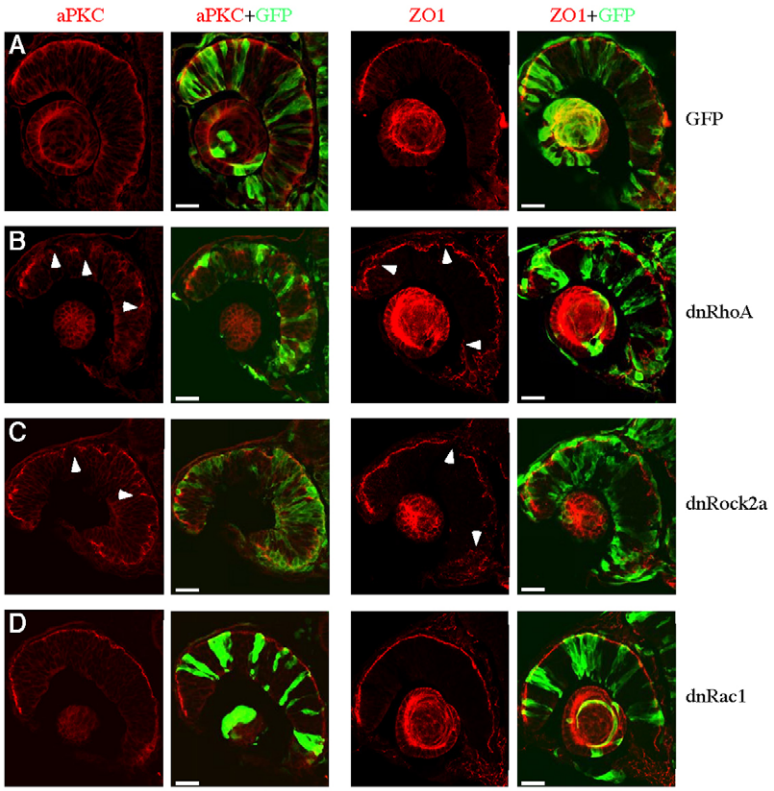

Fig. 7. RhoA and Rock2 but not Rac1 regulate polarity and morphogenesis of retinal progenitor cells. (**A-D**) Representative examples of confocal transverse sections of embryos at stage 25 expressing GFP (A), dominant-negative RhoA (B), dominant-negative Rock2 (C) or dominant-negative Rac1 (D). Expressing cells are labeled with GFP (green). Cells expressing dominant-negative RhoA (B) and dominant-negative Rock2 (C) are morphologically abnormal. TJ (arrowheads in column ZO1 of B,C) and aPKC (arrowheads in column aPKC of B,C) are mislocalized or absent. Cell morphology, aPKC and ZO1 localization are not affected by dominant-negative Rac1 expression (D). Scale bars: 25 μm.

actin modulates the pathway, leading to overgrowth (Sansores-Garcia et al., 2011). Thus, also perturbations of the actin cytoskeleton by loss of *ArhGEF18* function may modulate Hippo signaling and therefore perturb control of proliferation in RPCs.

Our results indicate that ArhGEF18 mediated activation of RhoA-Rock2 signaling is required for the maintenance rather than establishment of apicobasal polarity. Mutant embryos are initially phenotypically normal. Prior to the onset of differentiation, ArhGEF18 protein levels are low (1 dpf) and a marked increase is detectable at 2 dpf concomitant with the appearance of the mutant phenotype. Furthermore, we found that at later stages (4 dpf) newly formed RPCs in the CMZ are much less severely affected than older differentiating cells of the central retina.

Initially, *med* RPCs show normal columnar morphology. Subsequent to gradual mislocalization of TJ, mutant cells eventually adopt abnormal rounded morphologies and the epithelial arrangement deteriorates. Thus, loss of *ArhGEF18* function initially affects the a-b polarity of RPCs and as a consequence their morphology. Mutations of zebrafish aPKC similarly affect RPC morphology and a-b polarity (Horne-Badovinac et al., 2001). In addition, adherence junctions initially form and mutant RPCs are morphologically normal. Later, adherence junctions are not maintained and RPC morphology is abnormal and rounded. Thus, cellular morphology and epithelial organization depend on maintained a-b polarity.

Our analysis of mosaic tissue showed that single mutant cells behave cell non-autonomously in wild-type tissue, whereas larger mutant clones behaved cell autonomously. A dependence of clone size on cell behavior has also been reported for zebrafish *moe*, where single mutant photoreceptors were morphologically normal and larger clones exhibited mutant morphology (Jensen et al., 2001). A similar community effect was also observed for cytoskeletal polarization and mitosis orientation of progenitor cells in the zebrafish neural tube (Žigman et al., 2011). Steric constraints of surrounding wild-type tissue may influence the morphology of single mutant cells. However, aPKC was normally localized in single transplanted *med* mutant photoreceptors, indicative of normal a-b polarity. This suggests that mutant cells can respond correctly to signals provided by neighboring wild-type cells. In larger clones, these signals are lacking because of abutting mutant cells, leading to a mutant phenotype. Thus, our findings underscore the importance of cell signaling for epithelial polarity.

The genotype of RPE cells is not decisive for the phenotype of abutting RPCs, as wild-type RPE cannot rescue the underlying neuroretina and mutant RPE does not affect the normal underlying retina. Thus, ArhGEF18 regulated Rho-Rock signaling is required in the neuroretina as an intra-tissue mechanism to maintain epithelial polarity. This is in contrast to proteins of the apical Crbs complex, Moe and Nok, that are required in RPE cells and regulate a-b polarity of the underlying neural retina (Jensen et al., 2001; Wei and Malicki, 2002; Zou et al., 2008), thus acting in inter-tissue signaling within the developing eye.

In summary, we show that *ArhGEF18* regulates morphology, polarity and proliferation of the retinal neuroepithelium. Our results indicate that activation of the RhoA-Rock2 signaling pathway by ArhGEF18 is required for these processes. We therefore identify an important role for RhoA signaling in regulating a-b polarity and proliferation in vertebrate neuroepithelia, and delineate the underlying molecular pathway.

Acknowledgements
We thank Matthias Carl, Nicholas Foulkes, Clemens Grabher, Olivier Kassel, Juan Martinez-Morales and Lucia Poggi for critical reading of the manuscript. We acknowledge the excellent animal husbandry of Nadia Wolf, Nadine Eschen, Natalja Kusminski and Susanne Delong. Takahiro Nagase, Alexander Reugels, Lilianna Solnica-Krezel and Michael Way provided plasmids.

Funding
J.W. was supported by the Deutsche Forschungsgemeinschaft collaborative research center SFB488.

Competing interests statement
The authors declare no competing financial interests.

Author contributions
The mutations were cloned by F.L. in the lab of J.W. with technical assistance of C.M. and R.Q. The functional characterization was planned and carried out by F.L. and C.H. in F.L.'s lab. J.M.S. carried out the activation assay in the department of S.O. with his support. R.P. provided the statistical analysis and algorithm development. F.L. wrote the manuscript with the assistance of J.W.

Supplementary material
Supplementary material available online at
http://dev.biologists.org/lookup/suppl/doi:10.1242/dev.096487/-/DC1

References
Bao, Y., Hata, Y., Ikeda, M. and Withanage, K. (2011). Mammalian Hippo pathway: from development to cancer and beyond. *J. Biochem.* **149**, 361-379.
Barberis, D., Casazza, A., Sordella, R., Corso, S., Artigiani, S., Settleman, J., Comoglio, P. M. and Tamagnone, L. (2005). p190 Rho-GTPase activating protein associates with plexins and it is required for semaphorin signalling. *J. Cell Sci.* **118**, 4689-4700.
Benard, V., Bohl, B. P. and Bokoch, G. M. (1999). Characterization of rac and cdc42 activation in chemoattractant-stimulated human neutrophils using a novel assay for active GTPases. *J. Biol. Chem.* **274**, 13198-13204.
Blechinger, S. R., Evans, T. G., Tang, P. T., Kuwada, J. Y., Warren, J. T., Jr and Krone, P. H. (2002). The heat-inducible zebrafish hsp70 gene is expressed during normal lens development under non-stress conditions. *Mech. Dev.* **112**, 213-215.
Blomquist, A., Schwörer, G., Schablowski, H., Psoma, A., Lehnen, M., Jakobs, K. H. and Rümenapp, U. (2000). Identification and characterization of a novel Rho-specific guanine nucleotide exchange factor. *Biochem. J.* **352**, 319-325.
Del Bene, F., Ettwiller, L., Skowronska-Krawczyk, D., Baier, H., Matter, J.-M., Birney, E. and Wittbrodt, J. (2007). In vivo validation of a computationally predicted conserved Ath5 target gene set. *PLoS Genet.* **3**, e159.
Furutani-Seiki, M., Sasado, T., Morinaga, C., Suwa, H., Niwa, K., Yoda, H., Deguchi, T., Hirose, Y., Yasuoka, A., Henrich, T. et al. (2004). A systematic genome-wide screen for mutations affecting organogenesis in Medaka, Oryzias latipes. *Mech. Dev.* **121**, 647-658.
Halder, G. and Johnson, R. L. (2011). Hippo signaling: growth control and beyond. *Development* **138**, 9-22.
Hartsock, A. and Nelson, W. J. (2008). Adherens and tight junctions: structure, function and connections to the actin cytoskeleton. *Biochim. Biophys. Acta* **1778**, 660-669.
Heasman, S. J. and Ridley, A. J. (2008). Mammalian Rho GTPases: new insights into their functions from in vivo studies. *Nat. Rev. Mol. Cell Biol.* **9**, 690-701.
Herzog, D., Loetscher, P., van Hengel, J., Knüsel, S., Brakebusch, C., Taylor, V., Suter, U. and Relvas, J. B. (2011). The small GTPase RhoA is required to maintain spinal cord neuroepithelium organization and the neural stem cell pool. *J. Neurosci.* **31**, 5120-5130.
Horne-Badovinac, S., Lin, D., Waldron, S., Schwarz, M., Mbamalu, G., Pawson, T., Jan, Y., Stainier, D. Y. and Abdelilah-Seyfried, S. (2001). Positional cloning of heart and soul reveals multiple roles for PKC lambda in zebrafish organogenesis. *Curr. Biol.* **11**, 1492-1502.
Iwamatsu, T. (2004). Stages of normal development in the medaka Oryzias latipes. *Mech. Dev.* **121**, 605-618.
Jensen, A. M. and Westerfield, M. (2004). Zebrafish mosaic eyes is a novel FERM protein required for retinal lamination and retinal pigmented epithelial tight junction formation. *Curr. Biol.* **14**, 711-717.
Jensen, A. M., Walker, C. and Westerfield, M. (2001). Mosaic eyes: a zebrafish gene required in pigmented epithelium for apical localization of retinal cell division and lamination. *Development* **128**, 95-105.
Karnoub, A. E., Worthylake, D. K., Rossman, K. L., Pruitt, W. M., Campbell, S. L., Sondek, J. and Der, C. J. (2001). Molecular basis for Rac1 recognition by guanine nucleotide exchange factors. *Nat. Struct. Biol.* **8**, 1037-1041.
Katayama, K.-I., Melendez, J., Baumann, J. M., Leslie, J. R., Chauhan, B. K., Nemkul, N., Lang, R. A., Kuan, C.-Y., Zheng, Y. and Yoshida, Y. (2011). Loss of RhoA in neural progenitor cells causes the disruption of adherens junctions and hyperproliferation. *Proc. Natl. Acad. Sci. USA* **108**, 7607-7612.
Loosli, F., Köster, R. W., Carl, M., Kühnlein, R., Henrich, T., Mücke, M., Krone, A. and Wittbrodt, J. (2000). A genetic screen for mutations affecting embryonic development in medaka fish (Oryzias latipes). *Mech. Dev.* **97**, 133-139.
Loosli, F., Del Bene, F., Quiring, R., Rembold, M., Martinez-Morales, J.-R., Carl, M., Grabher, C., Iquel, C., Krone, A., Wittbrodt, B. et al. (2004). Mutations affecting retina development in Medaka. *Mech. Dev.* **121**, 703-714.
Luo, J., Uribe, R. A., Hayton, S., Calinescu, A.-A., Gross, J. M. and Hitchcock, P. F. (2012). Midkine-A functions upstream of Id2a to regulate cell cycle kinetics in the developing vertebrate retina. *Neural Dev.* **7**, 33.
Malicki, J. (2004). Cell fate decisions and patterning in the vertebrate retina: the importance of timing, asymmetry, polarity and waves. *Curr. Opin. Neurobiol.* **14**, 15-21.
Marlow, F., Topczewski, J., Sepich, D. and Solnica-Krezel, L. (2002). Zebrafish Rho kinase 2 acts downstream of Wnt11 to mediate cell polarity and effective convergence and extension movements. *Curr. Biol.* **12**, 876-884.
Martinez-Morales, J.-R., Naruse, K., Mitani, H., Shima, A. and Wittbrodt, J. (2004). Rapid chromosomal assignment of medaka mutants by bulked segregant analysis. *Gene* **329**, 159-165.
Martinez-Morales, J.-R., Rembold, M., Greger, K., Simpson, J. C., Brown, K. E., Quiring, R., Pepperkok, R., Martin-Bermudo, M. D., Himmelbauer, H. and Wittbrodt, J. (2009). Ojoplano-mediated basal constriction is essential for optic cup morphogenesis. *Development* **136**, 2165-2175.
Matsui, T., Raya, A., Kawakami, Y., Callol-Massot, C., Capdevila, J., Rodríguez-Esteban, C. and Izpisúa Belmonte, J. C. (2005). Noncanonical Wnt signaling regulates midline convergence of organ primordia during zebrafish development. *Genes Dev.* **19**, 164-175.
Nagata, K.-I. and Inagaki, M. (2005). Cytoskeletal modification of Rho guanine nucleotide exchange factor activity: identification of a Rho guanine nucleotide exchange factor as a binding partner for Sept9b, a mammalian septin. *Oncogene* **24**, 65-76.
Nakajima, H. and Tanoue, T. (2011). Lulu2 regulates the circumferential actomyosin tensile system in epithelial cells through p114RhoGEF. *J. Cell Biol.* **195**, 245-261.
Niu, J., Profirovic, J., Pan, H., Vaiskunaite, R. and Voyno-Yasenetskaya, T. (2003). G Protein betagamma subunits stimulate p114RhoGEF, a guanine nucleotide exchange factor for RhoA and Rac1: regulation of cell shape and reactive oxygen species production. *Circ. Res.* **93**, 848-856.
Oleksy, A., Opaliński, Ł., Derewenda, U., Derewenda, Z. S. and Otlewski, J. (2006). The molecular basis of RhoA specificity in the guanine nucleotide exchange factor PDZ-RhoGEF. *J. Biol. Chem.* **281**, 32891-32897.
Omori, Y. and Malicki, J. (2006). oko meduzy and related crumbs genes are determinants of apical cell features in the vertebrate embryo. *Curr. Biol.* **16**, 945-957.
Panizzi, J. R., Jessen, J. R., Drummond, I. A. and Solnica-Krezel, L. (2007). New functions for a vertebrate Rho guanine nucleotide exchange factor in ciliated epithelia. *Development* **134**, 921-931.
Poggi, L., Vitorino, M., Masai, I. and Harris, W. A. (2005). Influences on neural lineage and mode of division in the zebrafish retina in vivo. *J. Cell Biol.* **171**, 991-999.
Popoff, M. R. and Geny, B. (2009). Multifaceted role of Rho, Rac, Cdc42 and Ras in intercellular junctions, lessons from toxins. *Biochim. Biophys. Acta* **1788**, 797-812.
Pujic, Z. and Malicki, J. (2001). Mutation of the zebrafish glass onion locus causes early cell-nonautonomous loss of neuroepithelial integrity followed by severe neuronal patterning defects in the retina. *Dev. Biol.* **234**, 454-469.
Randlett, O., Norden, C. and Harris, W. A. (2011). The vertebrate retina: a model for neuronal polarization in vivo. *Dev. Neurobiol.* **71**, 567-583.
Rembold, M., Lahiri, K., Foulkes, N. S. and Wittbrodt, J. (2006a). Transgenesis in fish: efficient selection of transgenic fish by co-injection with a fluorescent reporter construct. *Nat. Protoc.* **1**, 1133-1139.
Rembold, M., Loosli, F., Adams, R. J. and Wittbrodt, J. (2006b). Individual cell migration serves as the driving force for optic vesicle evagination. *Science* **313**, 1130-1134.
Ren, X. D. and Schwartz, M. A. (2000). Determination of GTP loading on Rho. *Methods Enzymol.* **325**, 264-272.
Riento, K. and Ridley, A. J. (2003). Rocks: multifunctional kinases in cell behaviour. *Nat. Rev. Mol. Cell Biol.* **4**, 446-456.
Rossman, K. L., Worthylake, D. K., Snyder, J. T., Siderovski, D. P., Campbell, S. L. and Sondek, J. (2002). A crystallographic view of interactions between Dbs and Cdc42: PH domain-assisted guanine nucleotide exchange. *EMBO J.* **21**, 1315-1326.
Rossman, K. L., Der, C. J. and Sondek, J. (2005). GEF means go: turning on RHO GTPases with guanine nucleotide-exchange factors. *Nat. Rev. Mol. Cell Biol.* **6**, 167-180.
Royer, C. and Lu, X. (2011). Epithelial cell polarity: a major gatekeeper against cancer? *Cell Death Differ.* **18**, 1470-1477.
Samarin, S. and Nusrat, A. (2009). Regulation of epithelial apical junctional complex by Rho family GTPases. *Front. Biosci.* **14**, 1129-1142.
Sansores-Garcia, L., Bossuyt, W., Wada, K.-I., Yonemura, S., Tao, C., Sasaki, H. and Halder, G. (2011). Modulating F-actin organization induces organ growth by affecting the Hippo pathway. *EMBO J.* **30**, 2325-2335.

Souren, M., Martinez-Morales, J.-R., Makri, P., Wittbrodt, B. and Wittbrodt, J. (2009). A global survey identifies novel upstream components of the Ath5 neurogenic network. *Genome Biol.* **10**, R92.

Szymczak, A. L., Workman, C. J., Wang, Y., Vignali, K. M., Dilioglou, S., Vanin, E. F. and Vignali, D. A. A. (2004). Correction of multi-gene deficiency in vivo using a single 'self-cleaving' 2A peptide-based retroviral vector. *Nat. Biotechnol.* **22**, 589-594.

Tawk, M., Araya, C., Lyons, D. A., Reugels, A. M., Girdler, G. C., Bayley, P. R., Hyde, D. R., Tada, M. and Clarke, J. D. W. (2007). A mirror-symmetric cell division that orchestrates neuroepithelial morphogenesis. *Nature* **446**, 797-800.

Terry, S. J., Zihni, C., Elbediwy, A., Vitiello, E., Leefa Chong San, I. V., Balda, M. S. and Matter, K. (2011). Spatially restricted activation of RhoA signalling at epithelial junctions by p114RhoGEF drives junction formation and morphogenesis. *Nat. Cell Biol.* **13**, 159-166.

Wei, X. and Malicki, J. (2002). nagie oko, encoding a MAGUK-family protein, is essential for cellular patterning of the retina. *Nat. Genet.* **31**, 150-157.

Worthylake, D. K., Rossman, K. L. and Sondek, J. (2000). Crystal structure of Rac1 in complex with the guanine nucleotide exchange region of Tiam1. *Nature* **408**, 682-688.

Yamaguchi, M., Imai, F., Tonou-Fujimori, N. and Masai, I. (2010). Mutations in N-cadherin and a Stardust homolog, Nagie oko, affect cell-cycle exit in zebrafish retina. *Mech. Dev.* **127**, 247-264.

Žigman, M., Trinh, A., Fraser, S. E. and Moens, C. B. (2011). Zebrafish neural tube morphogenesis requires Scribble-dependent oriented cell divisions. *Curr. Biol.* **21**, 79-86.

Zou, J., Lathrop, K. L., Sun, M. and Wei, X. (2008). Intact retinal pigment epithelium maintained by Nok is essential for retinal epithelial polarity and cellular patterning in zebrafish. *J. Neurosci.* **28**, 13684-13695.

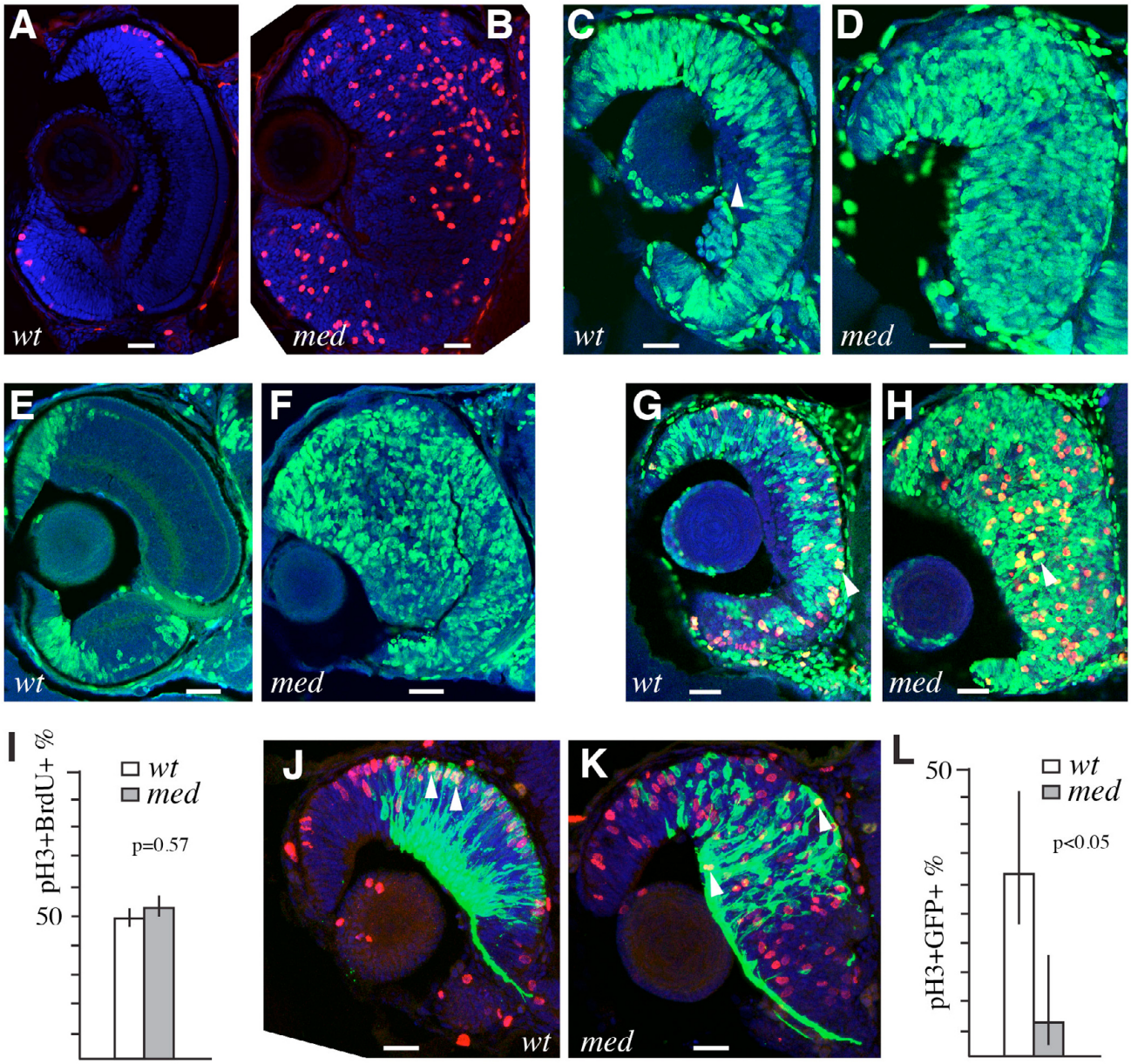

Fig. S1. Proliferation and cell cycle exit are affected by the *med* mutation. (**A**,**B**) M-phase nuclei are visualized by α-pH3 labeling in wild-type (A) and mutant (B) 4 dpf retinae. The central retina of the wild type, where differentiating neurons reside, is free of pH3 labeling. In the mutant, pH3 labeling is detectable in all regions and the ratio of pH3-positive nuclei is increased (see Fig. 1G). (**C**,**D**) BrdU labeling for 2 hours in wild-type (C) and mutant (D) retinae at 2.8 dpf. In the wild type, a small region of the central retina, where presumptive ganglion cells are differentiating, is free of BrdU labeling (arrowhead), whereas the mutant retina is ubiquitously labeled. (**E**,**F**) BrdU incorporation for 12 hours starting at 4 dpf. In the wild type (E), BrdU incorporation is restricted to the peripheral retina where proliferating RPCs reside, whereas in the mutant BrdU incorporation is detectable in all regions of the retina. (**G**,**H**) BrdU (green) and pH3 (red) double labeling at stage 27 to examine S- to M-phase cell cycle progression. BrdU was injected at stage 27 and after 9 hours embryos were fixed and stained for pH3 and BrdU. Examples of double-positive nuclei (yellow) are indicated (arrowheads). (**I**) The ratio of pH3 and BrdU double-positive to total pH3-positive nuclei was analyzed to determine the relative number of cells that progress from S to M phase during the 9 hours of BrdU incorporation. This ratio is similar in both wild type and mutant, indicating that cell cycle progression proceeds normally in mutant RPCs. (**J**,**K**) The expression of ath5 was used to visualize RPCs undergoing the final cell division prior to neuronal differentiation (Poggi et al., 2005; Yamaguchi et al., 2010) by crossing a stable transgenic line expressing GFP under the control of the ath5 regulatory region [ath5::GFP (del Bene et al., 2007)] into the *med* mutant. In this context, cells undergoing a neurogenic division are positive for both pH3 (red, M phase) and GFP (green, ath5). In both mutant and wild type, GFP expression was first detectable in central RPCs at stage 26 and subsequently spread across the retina to more peripheral regions (del Bene et al., 2007) (data not shown). This indicates that neurogenesis is normally initiated in the mutant retina. At stage 27, we quantified the ratio of pH3/GFP double-positive nuclei (arrowhead) to total pH3 nuclei to analyse cell cycle exit. (**L**) Quantification the ratio of pH3/GFP double-positive to total pH3-positive cells to analyze the relative number of cells exiting the cell cycle by neurogenic divisions. In the wild type, 33% of the pH3-positive cells are also GFP positive, in the mutant this ratio is significantly reduced to 6.8%, indicating an almost fivefold reduction of cell cycle exit. (A-H,J,K) Confocal transversal sections, nuclei are stained with DAPI (blue). Scale bars: 25 μm in A-H,J,K.

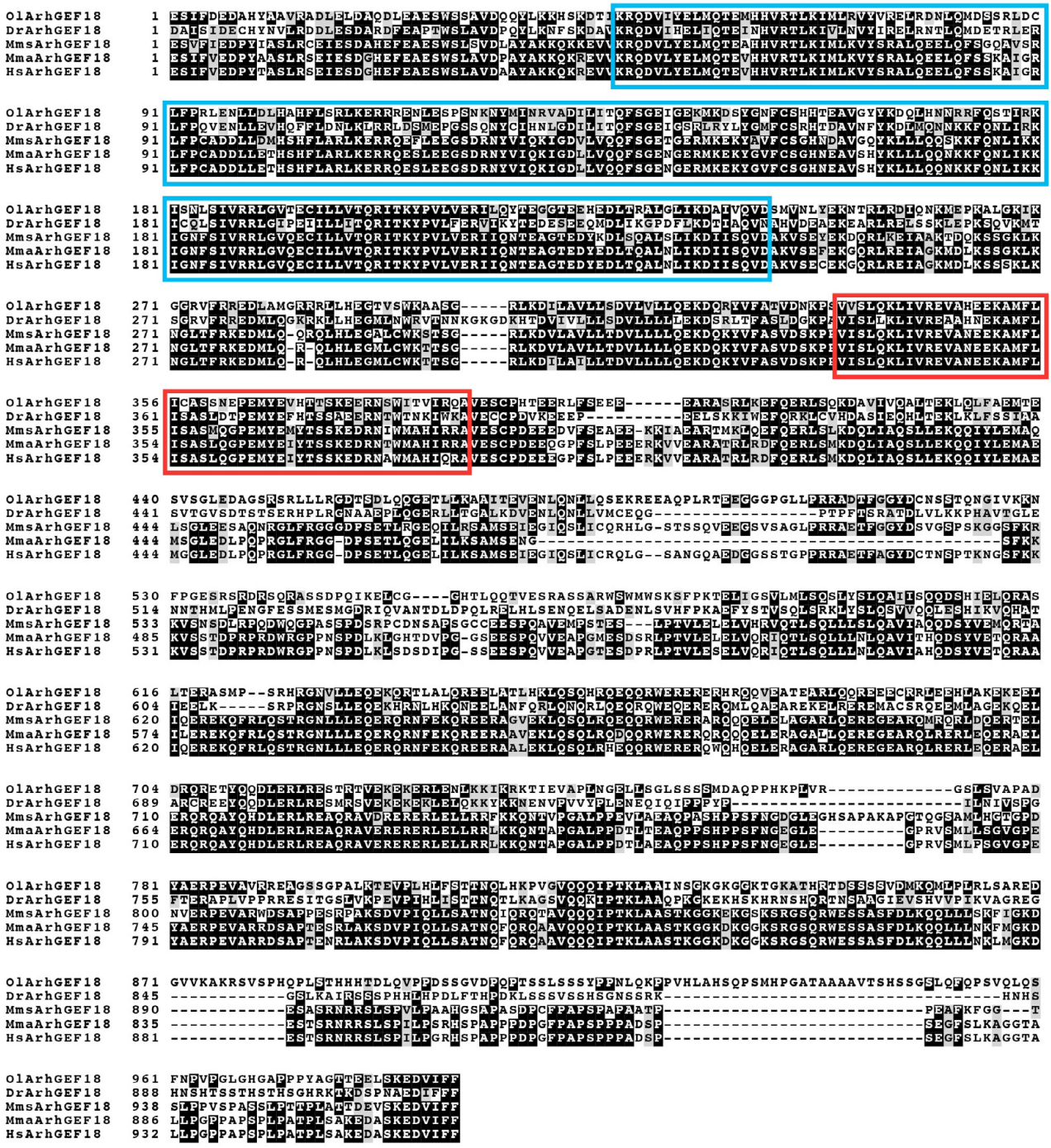

Fig. S2. Vertebrate ArhGEF18 homologues are conserved. Alignments of medaka (*Oryzias latipes*, OlArhGEF18: GenBank JN868075), zebrafish (*Danio rerio*, DrArhGEF18: Uniprot Q6NSP2), mouse (*Mus musculus*, MmsArhGEF18: GenBank EDL21902), macaca (*Macaca mulatta*, MmaArhGEF18: NCBI XP_001095927) and human (*Homo sapiens*, HsArhGEF18: NCBI NP_056133) proteins. The conserved DH (blue) and PH (red) domains are indicated. The DH domain is 60.2% identical to that of the zebrafish homologue and 65.8% to the DH domain of the murine and human homologue. The PH domain is 67.3 identical to that of zebrafish and 71.2% and 69.2% to that of mouse and humans, respectively. The C-terminal part of 604 amino acids is less well conserved, ranging from 39.5% (zebrafish) to 41.2% (human) identity.

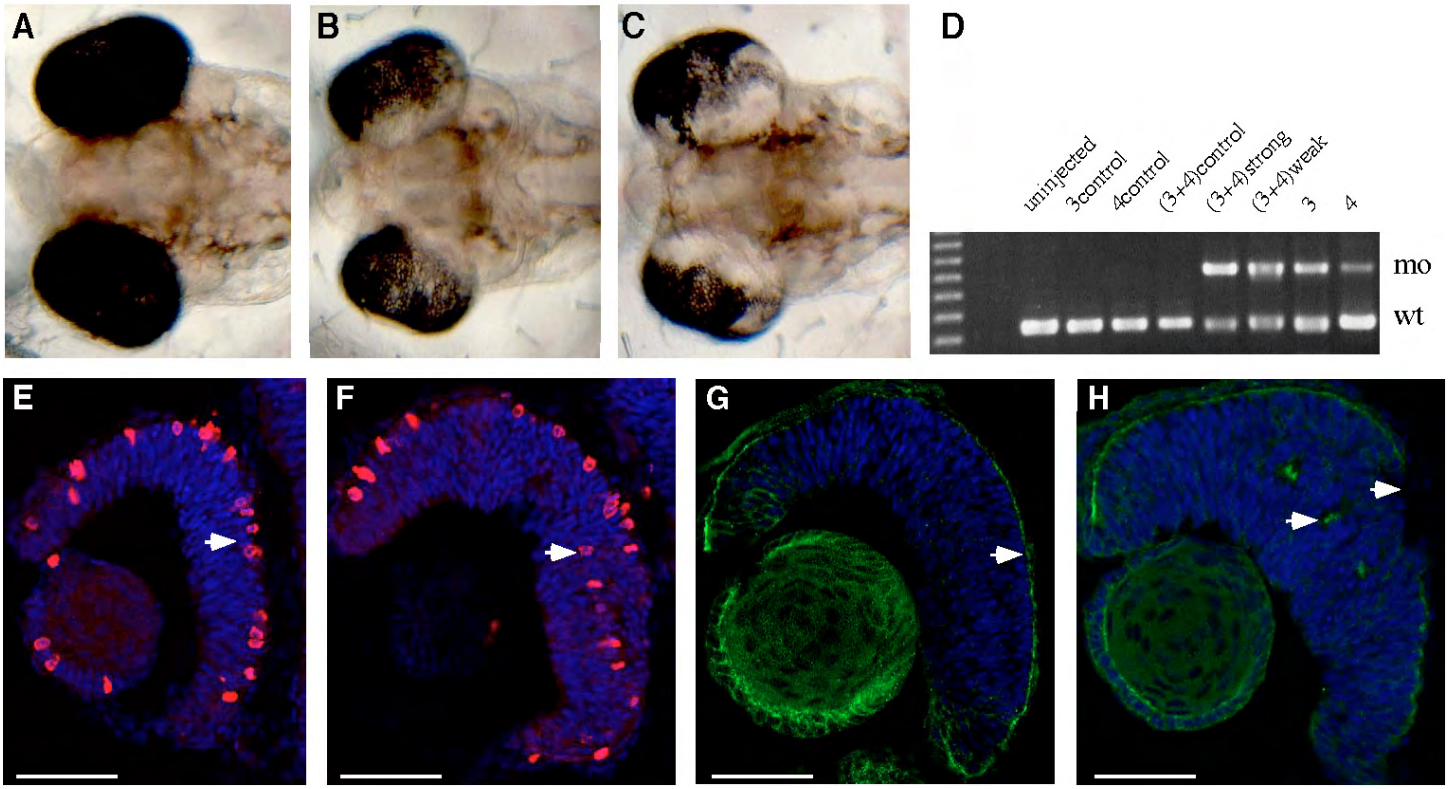

Fig. S3. *OlArhGEF18* morpholino injection phenocopies the *med* mutation. (**A-C**) Dorsal views of control-injected embryos (A), morpholino 3+4-injected embryos with weak phenotype (B) and morpholino 3+4-injected embryos with strong phenotype (C) at 4 dpf. (**D**) RT-PCR analysis of *OlArhGEF18* mRNA of morpholino and uninjected embryos. Uninjected and control morpholino-injected embryos show the wild-type transcript (lower band: wt); injection of morpholino 3, morpholino 4 and morpholino 3+4 results in splicing inhibition. The amount of unspliced transcript (upper band: mo) correlates with the severity of the phenotype. (**E**,**F**) Position of M-phase nuclei as visualized by α-PH3 antibody-labeling in control morpholino- (E) and morpholino 3+4- (F) injected embryos at stage 25 in the retina. Morpholino 3+4 injection results in mislocalized nuclei (F, arrowheads), whereas in the wild type, nuclei are apically localized (E). (**G**,**H**) aPKC localization in control morpholino- (G) and morpholino 3+4- (H) injected embryos at stage 27. Apical aPKC localization in the retina is severely perturbed in morpholino 3+4-injected embryos (arrowheads). (E-H) Nuclei are stained with DAPI (blue). Scale bars: 50 µm in E,F. Morpholino sequences: MO3, TGAATGCAAATGTGGGTGCTTACCA; MO3C, TCAATGGAAATCTGGGTCCTTAGCA; MO4, CAGCTCTGTGAGACGACACCAGTGT; MO4C, CACCTCTCTGACACGAGACCACTGT.

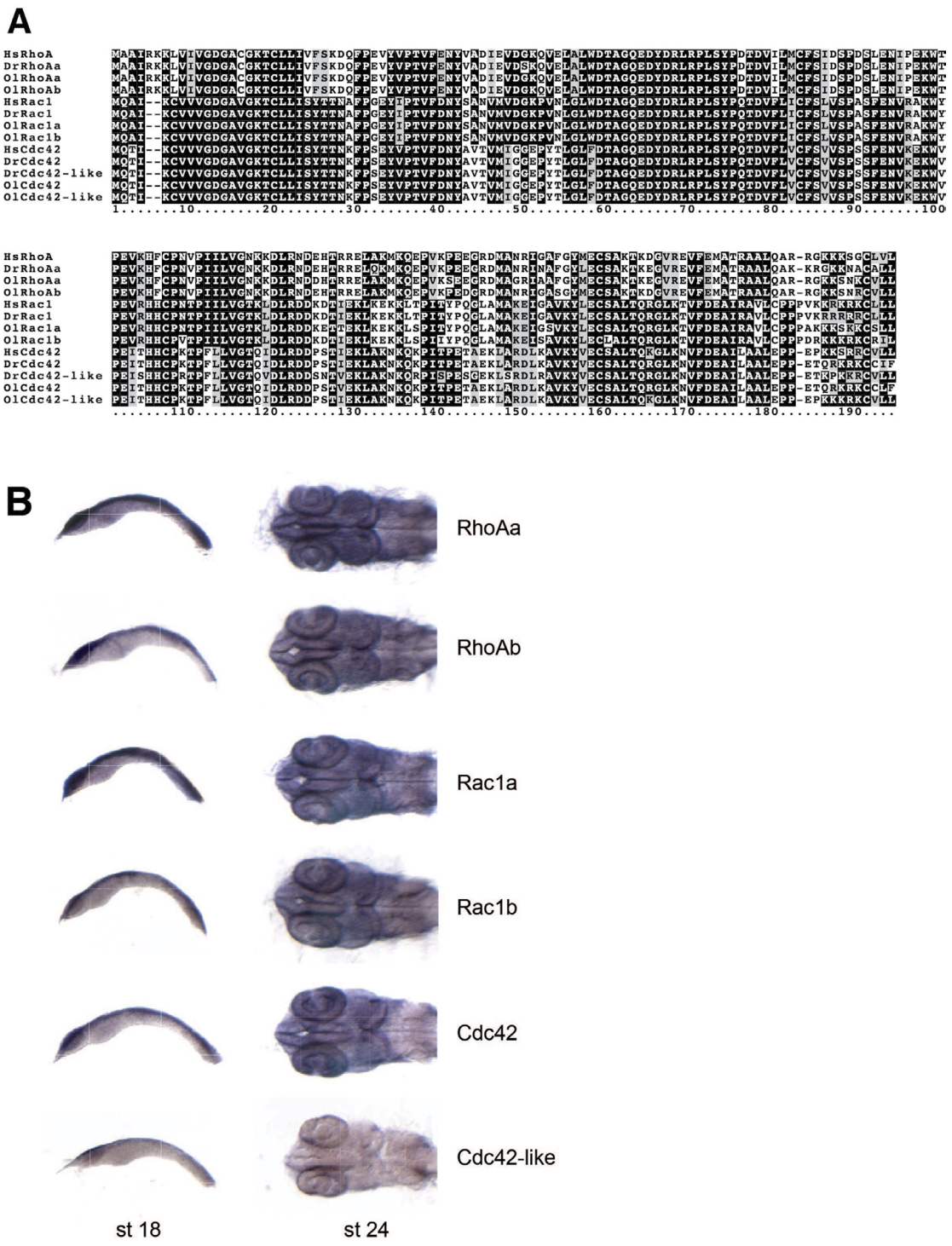

Fig. S4. Vertebrate RhoA, Rac1 and Cdc42 GTPases are highly conserved and ubiquitously expressed in medaka embryos at neurula and organogenesis stages. (**A**) Protein sequence comparison of human RhoA (Hs RhoA), Rac1 (HsRac1), Cdc42 (HsCdc42); zebrafish RhoAa (DrRhoAa), Rac1 (DrRac1), Cdc42 and Cdc42-like (DrCdc42, DrCdc42-like); and medaka RhoAa and RhoAb (OlRhoAa, OlRhoAb), Rac1a and Rac1b (OlRac1a, OlRac1b), and Cdc42 and Cdc42-like (OlCdc42, OlCdc42-like) are shown. Medaka RhoAa and RhoAb are 95% and 96% identical to human RhoA. Medaka Rac1a and Rac1b share 97% and 96% identity with human Rac1. Medaka Cdc42 and Cdc42-like are 96% and 99% identical, respectively, to human Cdc42. Most variable amino acids are located in the C-terminal region of the respective GTPases. All amino acids that have been implicated in GEF binding (Karnoub et al., 2001; Oleksy et al., 2006; Rossman et al., 2002; Worthylake et al., 2000) are completely conserved in these GTPases. OlRhoAa FOE002-P00007-DPE-F_I14 (GenBank: AM298929), OlRhoAb FOE002-P00007-DPE-F_M18 (GenBank: AM299029), OlRac1a FOE002-P00022-DPE-F_N10 (GenBank: AM304480), OlRac1b FOE002-P00013-DPE-F_P20 (GenBank: AM301286), OlCdc42 FOE002-P00024-DPE-F_A03 (GenBank: AM304876) and OlCdc42-like FOE002-P00008-DPE-F_C14 (GenBank: AM299156) were identified by BLAST searches from a medaka unigene cDNA library (Souren et al., 2009) using sequences of zebrafish homologues. (**B**) Whole-mount in situ hybridization expression analysis of *RhoAa*, *RhoAb*, *Rac1a*, *Rac1b*, *Cdc42* and *Cdc42-like* GTPases in wild-type medaka embryos at neurula (stage 18) and organogenesis (stage 24) stages. With the exception *of Cdc42-like*, all GTPases are ubiquitously expressed in the developing medaka embryo.

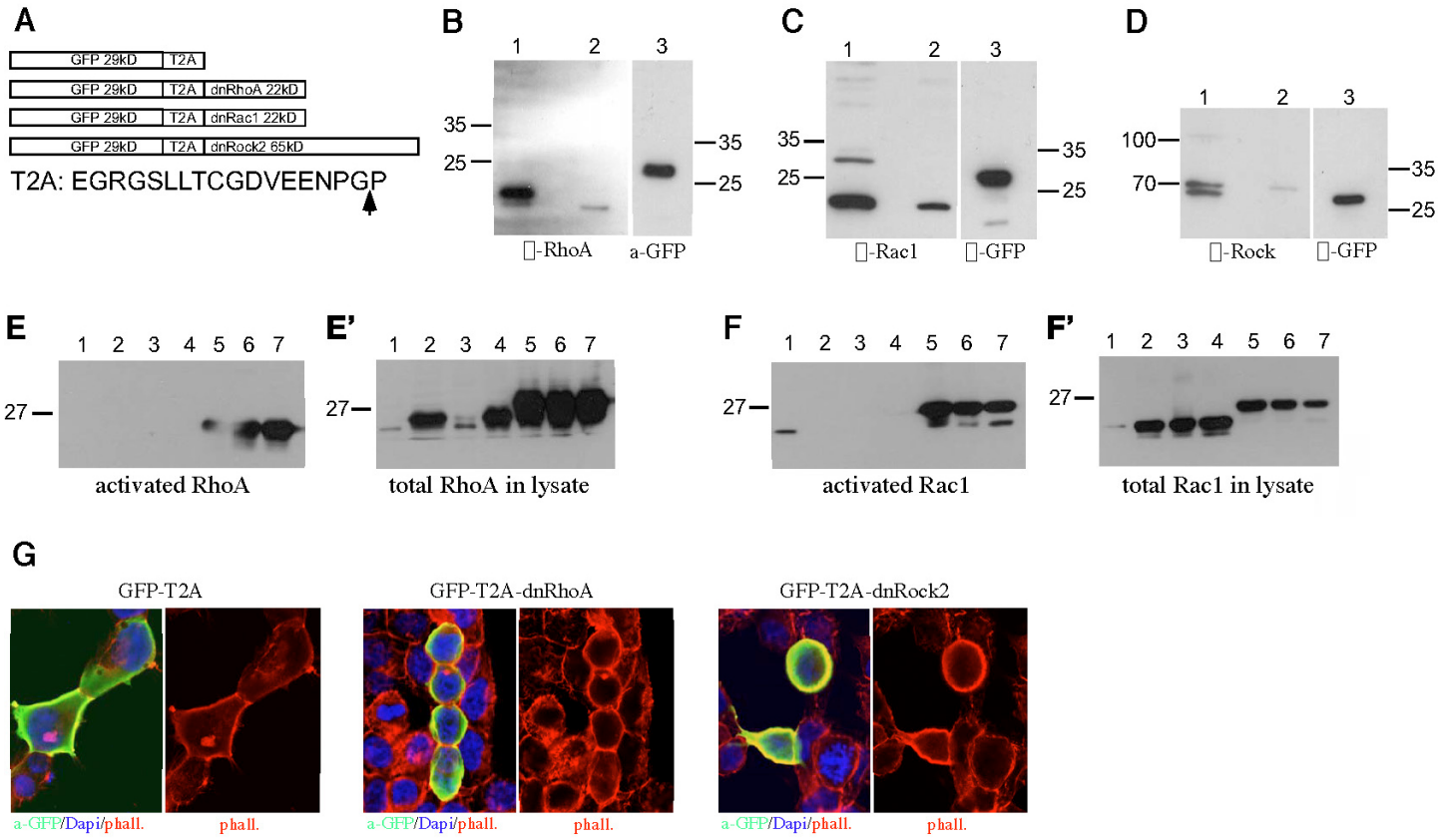

Fig. S5. T2A peptide separates GFP and a C-terminal polypeptide into two functional proteins. (**A**) Scheme of the GFP-T2A expression constructs. N-terminal GFP and the C-terminal dominant-negative protein were linked in-frame by the *Thosea asigna* virus T2A peptide, where a ribosomal skip mechanism results in the 'cleavage' of GFP and dominant-negative protein, respectively. This allows us to co-express these two proteins from a single vector (Szymczak et al., 2004). The expected sizes of the respective 'cleavage'-products in kDa is indicated. The amino acid sequence of the *Thosea asigna* virus T2A peptide and the 'cleavage'-site is shown. (**B-D**) Western blot analysis of 24 hpf medaka embryos injected at the one-cell stage with RNA encoding GFP-T2A-dominant-negative-RhoA (GFP-T2A-dnRhoA; B), GFP-T2A- dominant-negative-Rac1 (GFP-T2A-dnRac1; C) and GFP-T2A- dominant-negative-Rock2 (GFP-T2A-dnRock2; D). Lane 1, lysate of injected embryos probed with the indicated antibodies; lane 2, lysate of uninjected embryos probed with the indicated antibodies; lane 3, lysate of injected embryos probed with α-GFP antibody. The protein sizes are indicated in kDa. Expression of GFP-T2A-dnRhoA (B), GFP-T2A-dnRac1 (C) and GFP-T2A-dnRock2 (D) in medaka embryos results in the cleavage of GFP and the respective C terminal protein. (**E**,**F**) GTPase activation in HEK293 cells in response to GFP-T2A-dnRhoA and constitutive activated RhoA (E,E′) and GFP-T2A-dnRac1 and constitutive activated Rac1 (F,F′). Lanes are as follows: 1, untransfected; 2-4, GFP-T2A-dominant negative GTPase; 5-6, constitutive activated GTPase. (E) GFP-T2A-dnRhoA is inactive as determined by the absence of binding to GST-RBD (lanes 2-4), whereas activated RhoA strongly binds GST-RBD (lanes 5-7). (E′) Total amount of RhoA in the cell lysate. (F) GFP-T2A-dnRac1 is inactive as determined by the absence of binding to GST-Pak1 (lanes 2-4), whereas activated Rac1 shows strong binding. (F′) Total amount of Rac1 in the cell lysate. (**G**) HEK298 cells expressing GFP-T2A (negative control), GFP-T2A-dnRhoA and GFP-T2A-dnRock2 were stained for GFP (α-GFP) and actin (phalloidin), respectively. Cells expressing GFP-T2A-dnRhoA and GFP-T2A-dnRock2 delaminate and round up, thus indicating that dnRhoA and dnRock2 efficiently block RhoA and Rock2 activity, respectively (Barberis et al., 2005).

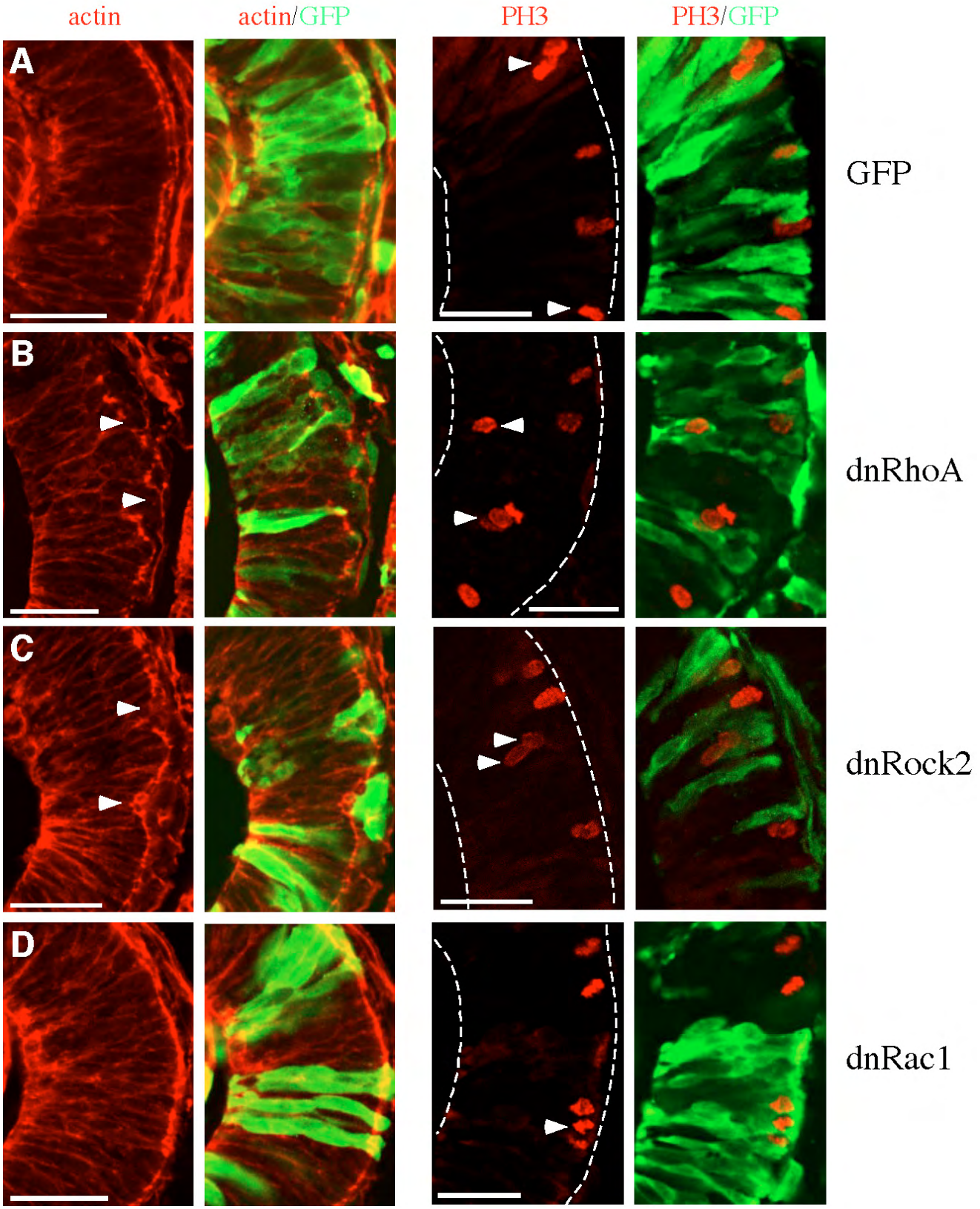

Fig. S6. RhoA and Rock2 but not Rac1 are required for cortical actin localization and apical localization of M-phase nuclei. (**A-D**) Representative examples of confocal transversal sections of embryos at stage 25 expressing GFP (A), dominant-negative RhoA (B), dominant-negative Rock2 (C) or dominant-negative Rac1 (D) under the control of a heat-shock promoter. Expressing cells are labeled with GFP (green). The retinal neuroepithelium is outlined by a broken line in column PH3. In cells expressing dominant-negative RhoA (B) and dominant-negative Rock2 (C) cortical actin localization is disturbed. Apical actin bundles are mislocalized or absent (arrowheads in column actin of B,C). In addition, apical localization of M-phase nuclei is affected by expression of dominant-negative RhoA (B) and dominant negative Rock2 (C). Nuclei of mitotic cells visualized by α-PH3 antibody staining are often displaced basally in expressing cells (arrowheads in column PH3 of B,C). Cortical actin localization and apical localization of M-phase nuclei are not affected by expression of dominant-negative Rac1 (D). Scale bars: 25 μm.